

Three-Dimensional Optimization of Blade Lean and Sweep for a Transonic Axial Compressor and Investigation of the On-Design and Off-Design Engine Performance

Mojtaba Heidarian Shahri, Ali Madadi*, Romina Ahadian

Department of Aerospace Engineering, Amirkabir University of Technology, Tehran, Iran

*Corresponding author's email: Ali.Madadi@aut.ac.ir

Abstract

Recently optimization methods have been considered by authors to enhance the turbo-machines performance. In this article, the genetic algorithm (GA) and artificial neural network (ANN) with computational fluid dynamics (CFD), are being coupled and the optimization of NASA Rotor-67, an axial compressor has simulated. The compressor flow field is simulated with CFD and the results proved the excellent validating with experimental data. The rotor leaned and swept parametrization was modeled and the results are improvements in design objective functions: pressure ratio, isentropic efficiency, and mass flow rate. According to the best-optimized case results, the mass flow rate, pressure ratio, and isentropic efficiency of the design point have been increased by about 2.020%, 1.297%, and 0.174%, respectively. Improving the convergence of surface streamlines in delaying the shock on the blade is another factor in improving the optimal rotor's performance compared to the base one. Then, the effect of the best-optimized rotor is studied at the on-design and off-design steady-state performance of a turbojet engine. The matching code has been worked by solving compatibility equations using the characteristic maps. The results show that Thrust has improved at design and off-design speeds.

Keywords

Compressor, Optimization, Artificial Intelligence, Lean and Sweep, Thermodynamic.

Nomenclature

a, b, d	Coefficients of c_p equation
c_p	Specific heat capacity at pressure constant
c_v	Specific heat capacity at volume constant
Eq	Equation
h	Enthalpy
l_1, l_2, l_3, l_4, l_5	Control points of spline algorithm for lean
$Imp.$	Improved
k	The ratio of specific heats
MW	Molecular weight
\dot{m}	Mass flow rate [kg/s]
NA	Not available
Obj	Objective function
$Opt.$	Optimized
PR	Pressure ratio
P	Pressure
R	Gas constant
s_1, s_2, s_3, s_4, s_5	Control points of spline algorithm for sweep
T	Temperature
x	Mole fraction
y	Mass fraction

Subscripts

D	Design
in	Inlet
is	Isentropic
mix	Mixture
out	Outlet
NS	Near stall
0	Stagnation property
ref	Reference
$univ$	Universal

Greek symbols

η	Isentropic Efficiency
δ	Displacement

1- Introduction

The performance enhancement of axial compressors, which are widely used in industries, has been a major challenge for engineers, requiring an interactive approach to parameters such as pressure ratio and performance efficiency. Three-dimensional geometric changes in compressor blades have been the primary means to achieve the desired results, achieved through targeted changes in leaned and swept blade. Examples of geometric changes in leaned and swept blade in compressors are mentioned below, where artificial intelligence coupled with computational fluid dynamics has yielded results. The authors also have studied some research in the numerical optimization and design of experiment (DOE) field of axial compressors, which has led to improvement in the surge margin and near stall isentropic efficiency of axial [1] and radial compressors [2].

A study on optimizing the leaned and swept blade of an axial compressor stage was conducted by Zhongyi et al, where optimal blade geometry was found through numerical optimization, resulting in the extraction of three near-stall design points and close-to-stall performance improvement, including improved isentropic efficiency and significant surge margin increase [3].

Research on geometric changes and achieving new performance from the LPC module of a turbofan engine was carried out by Eggers et al, considering the high-pressure distortion effects coming from the fan on its booster. Leaned and swept blade were also used to change the geometry of the booster inlet guide vanes, resulting in a pressure drop improvement of up to 18% [4].

In a study published by Hamaguchi et al, the effects of forward sweep on increasing the stability margin of a centrifugal compressor were evaluated, where the upstream flow distortion affects it. According to the extracted results, forward sweep effects have a significant impact on the surge margin and rotor stability [5].

The geometric modification of a swept impeller in the design point and off-design conditions has been studied by Li et al [6]. The modified sweep geometry includes a lower loss and pressure drop compared to the baseline geometry due to the displacement of shock formation on the impeller surface.

Benini studied NASA Rotor-37 geometry by genetic algorithm to aerodynamically optimize the blade stacking line [7, 8]. This paper aims to achieve a maximum of two target parameters, pressure ratio and isentropic efficiency at the design point, using lean and sweep concepts. TASKFLOW software has been used for numerical simulation. Results indicate a 5.5% increase in pressure ratio and only 0.08% decrease in isentropic efficiency.

The lean, sweep and end-bend effects on the aerodynamic performance of a transonic compressor (NASA Rotor-37) have been evaluated by Wang et al [9] by combining the numerical coupling method with the Shapley Additive Explanations (SHAP). The near-tip swept change has the most effects on efficiency.

The authors have previously conducted numerical research on three-dimensional optimization of axial fan and compressor using the lean and sweep methods [10, 11]. The numerical study of AGARD wing has been done similarly by authors with these process [12]. In the axial compressor studies that mentioned, a 3rd order polynomial equation was employed to parametrization the three-dimensional stacking-line of the axial rotor. The distinguishing feature and innovation presented in this paper is firstly the use of spline curves to represent significant changes in the rotor stacking-line, aimed at achieving lean and sweep variations to reach higher performance points than before. These steps are elaborated upon in the continuation of the research, forming its first part. Additionally, the second part of the paper includes an analysis of the thermodynamic cycle under off-design conditions. In this context, the performance results of the optimized compressor are examined within the engine cycle, derived from a developed in-house code. The use of various objective functions in the three-dimensional optimization loop of the rotor has enabled the attainment of points with increased mass flow rates while maintaining a constant design isentropic efficiency. This enhancement allows for greater performance generation in both on-design and off-design operating conditions within the thermodynamic cycle.

So in this study, it has been attempted to achieve superior rotors by simultaneously optimizing the blade sweep and lean on an axial rotor blade, which has previously been validated using numerical tools, in order to increase mass flow rate and pressure ratio. Therefore, the generated initial database has been sensitized and, with the help of neural network tools, the computational costs resulting from searching for the optimal point have been reduced, leading to the genetic algorithm. The use of geometric constraints for generating reliable geometries has significantly influenced and improved the marginal efficiency of these geometries. The results demonstrate the performance improvement of all rotor functions at the design and off-design points. Furthermore, due to investigating the effect of improving a component in the engine, the thermodynamic cycle performance (compatibility equations for steady-state conditions) has been obtained through the convergence of its compatibility equations. The results of this analysis compare the engine thrust force with the default rotor and optimized rotors, showing an improvement in engine thrust force.

2- CFD simulation of NASA Rotor-67

2-1- Test-case

CFD analysis of a NASA axial rotor test case has been selected to study and modify the geometry for performance improvement. This rotor is located in the first stage of an axial compressor (as shown in Fig. 1), and the aerodynamic characteristics at its design point are mapped in the Table 1. The available experimental results for this rotor are also data-mapped at two measurement locations used for validation with numerical data [13].

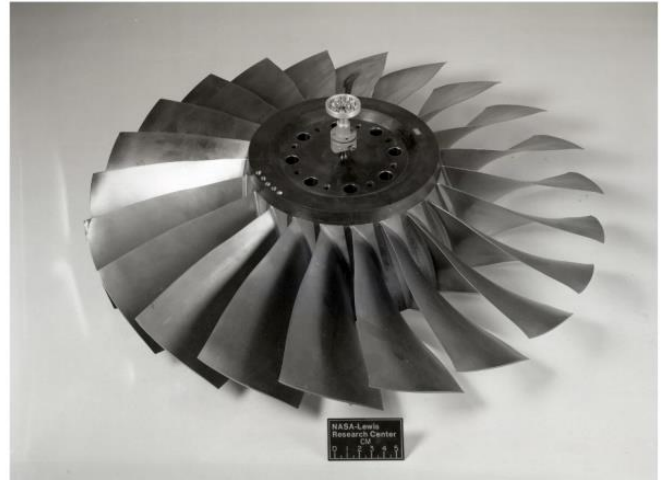
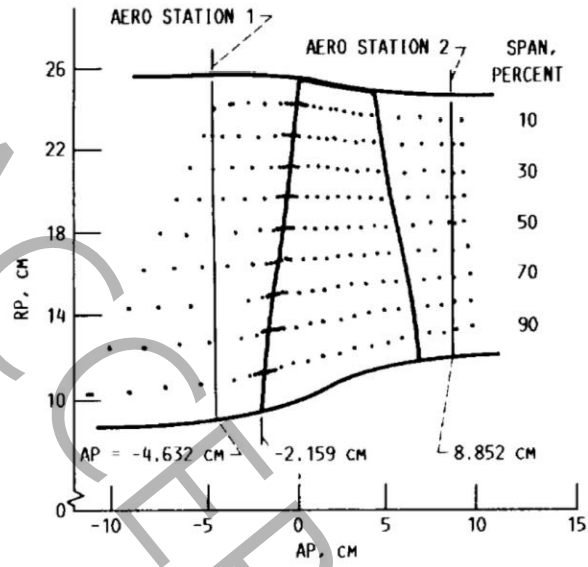


Fig. 1: NASA Rotor-67 at (a) meridional and (b) three-dimensional views [13]

Table 1: NASA Rotor-67 specification

Geometry specification	Number of blades	22
	Inlet tip diameter [cm]	51.4
	Exit tip diameter [cm]	48.5
	Inlet hub-to-tip radius ratio	0.375
	Exit hub-to-tip radius ratio	0.478
	Hub solidity	3.11
	Tip solidity	1.29
	Rotor aspect ratio	1.56
Performance values	Rotational speed [rpm]	16043
	Total pressure ratio	1.632
	Mass flow rate [kg/s]	33.794
	Adiabatic efficiency	0.919
	Inlet tip relative Mach number	1.38
	Tip speed [m/s]	429

Therefore, a structured three-dimensional mesh was used for analysis and characteristic curve extraction, as shown in Fig. 2. This mesh was employed for the aerodynamic field around a single-blade to reduce computational costs. Periodic boundary conditions around the walls have been used to aid in this process.

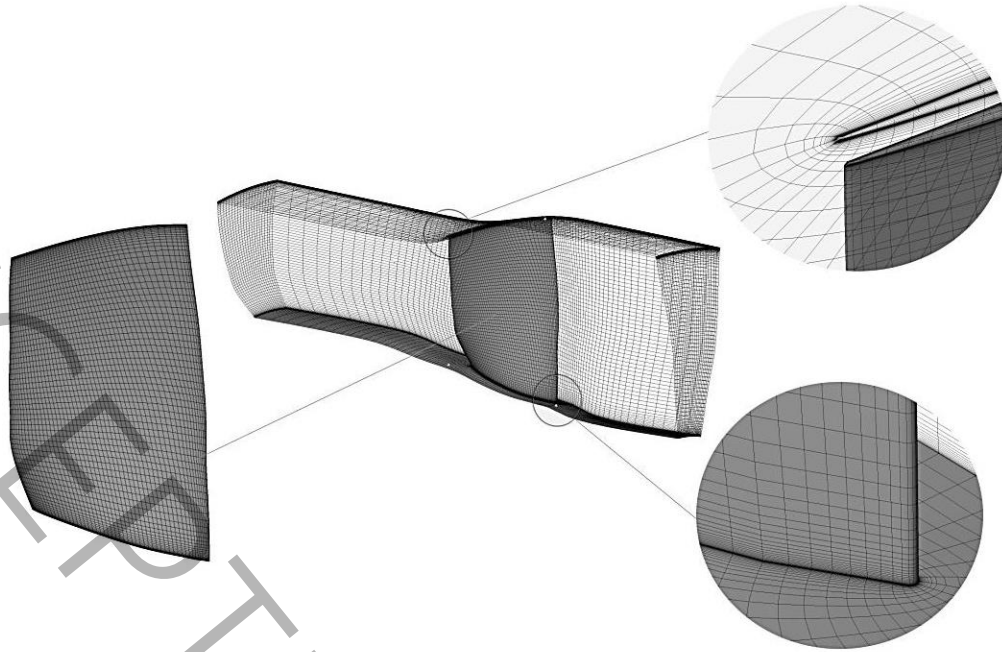


Fig. 2: Grids for NASA Rotor-67

2-2- Grid study

The grid study of characteristic data from the number of computational field elements, the grid count has been increased (480,000, 720,000, 1,360,000, and 1,780,000 elements) and the variations in shapes have been depicted in the Fig. 3.

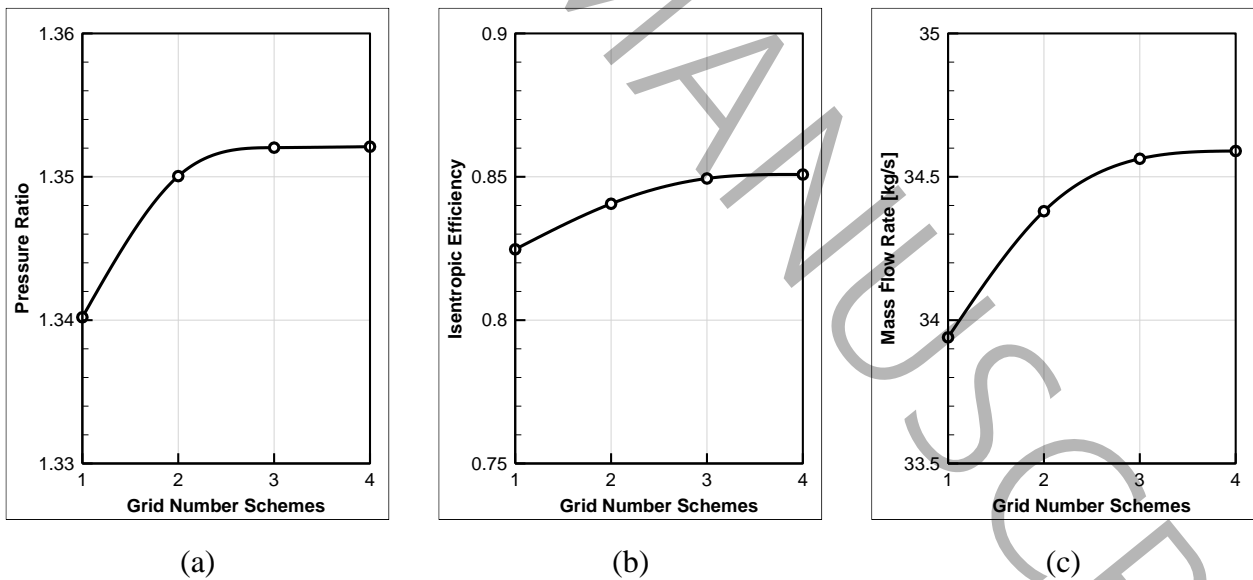


Fig. 3: Grid study of CFD results for (a) pressure ration, (b) isentropic efficiency, and (c) mass flow rate

The fine grid (Grid No.3), which involves subtle changes in performance results in an acceptable range for the Yplus number (as shown in Fig. 4) has been used in generating performance curves and validation.

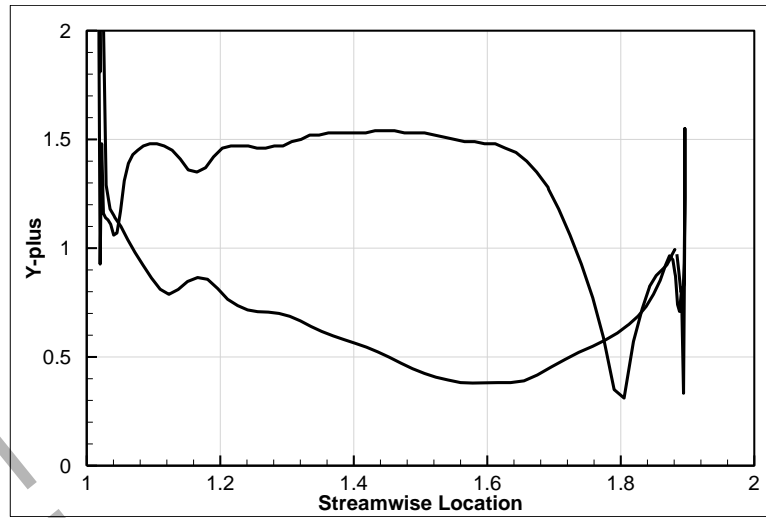


Fig. 4: NASA Rotor-67 Yplus distribution

The distribution of the Y-plus number along the blade length indicates that, although the local Y-plus values increase in the regions near the leading and trailing edges, the overall average Y-plus value along the blade length is approximately one, according to the studies conducted by the authors of this research. Therefore, this value is considered acceptable for other research analyses.

2-3- Validation

The three-dimensional computational fluid dynamics (CFD) simulation of the specified compressor domain has been defined as illustrated in the Fig. 5. To reduce computational costs, a single blade was utilized, incorporating both the inlet and outlet domains at its beginning and end.

Air enters the compressor under atmospheric conditions, and by varying the static pressure at the compressor's exit, the characteristic curve is extracted. The equations targeted in the analysis include momentum equations in three coordinate directions, the continuity equation, the energy equation, turbulence equations, and the ideal gas equation.

The numerical analysis employed the Shear Stress Transport (SST) turbulence model, with RANS equations converged to a precision of $1e-6$.

In near the compressor stall regions, where flow instability is more pronounced than in choked areas, the condition for complete convergence may not be satisfied. Therefore, the output pressure ratio was dynamically plotted to determine the cessation and convergence of the problem by stabilizing that parameter. The maximum number of convergence iterations was set to 500.

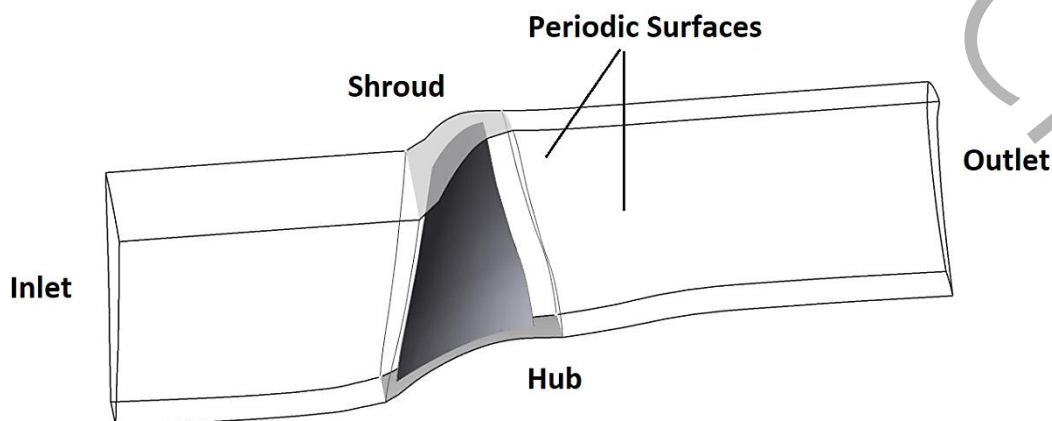


Fig. 5: Boundary conditions of Rotor-67 CFD simulation

The characteristic curve extracted at the design point using numerical methods has been compared with the reference experimental results and is depicted in Fig. 6.

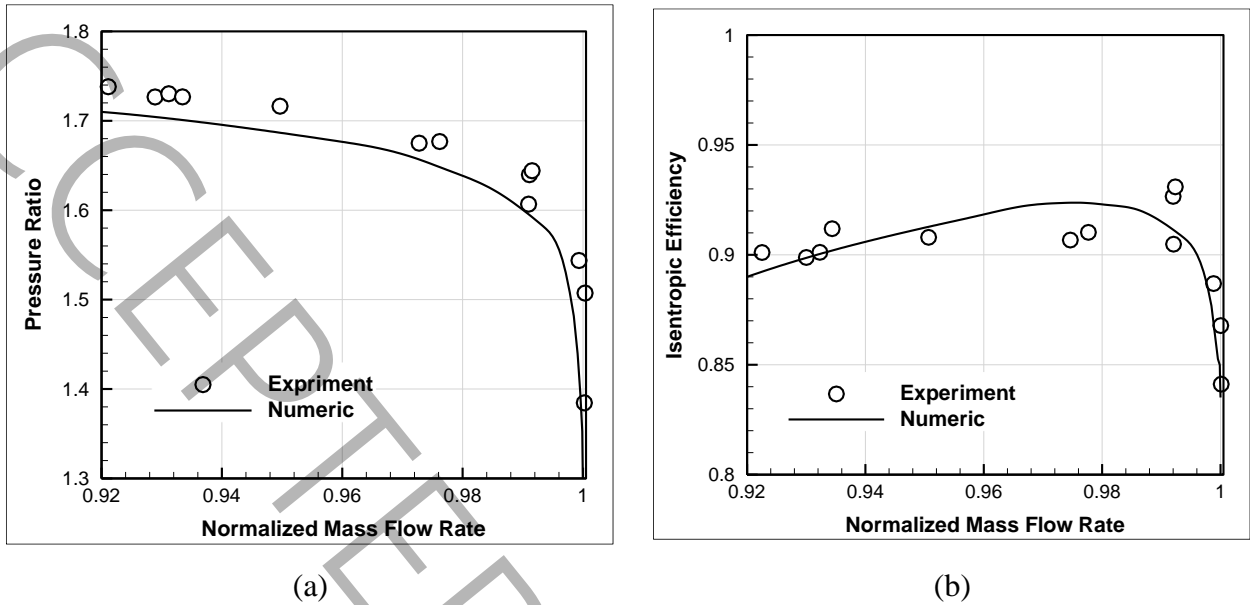


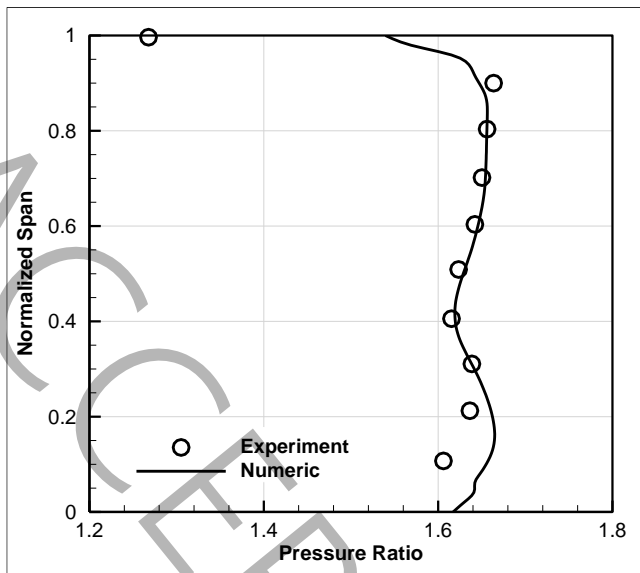
Fig. 6: Map Validation for (a) pressure ratio-mass flow rate, and (b) isentropic efficiency-mass flow rate

The comparison of performance values at the design point for the numerical method is presented in the Table 2. According to the obtained results, an acceptable level of accuracy has been achieved for the numerical results.

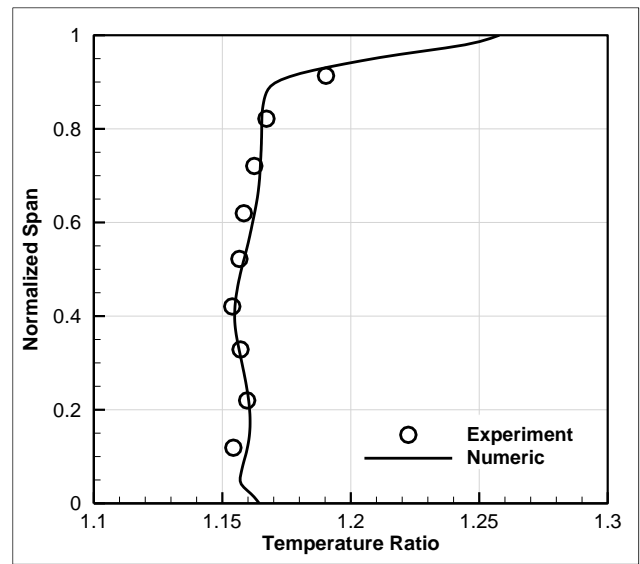
Table 2: Comparison of numerical results with experimental data at the design point

	Performance Parameters		
	Pressure Ratio	Isentropic Efficiency	Mass Flow Rate [kg/s]
Numerical	1.635	0.923	33.91
Experimental	1.632	0.919	33.79
Difference [%]	0.18 %	0.39 %	0.34 %

Furthermore, the distribution of pressure ratio and isentropic efficiency of the rotor at this design point has been extracted and compared with experimental test results in Fig. 7. The very good agreement results indicate the validation of numerical results. Therefore, the numerical tool used in this study can be an effective and efficient tool for predicting flow for optimal geometries.



(a)



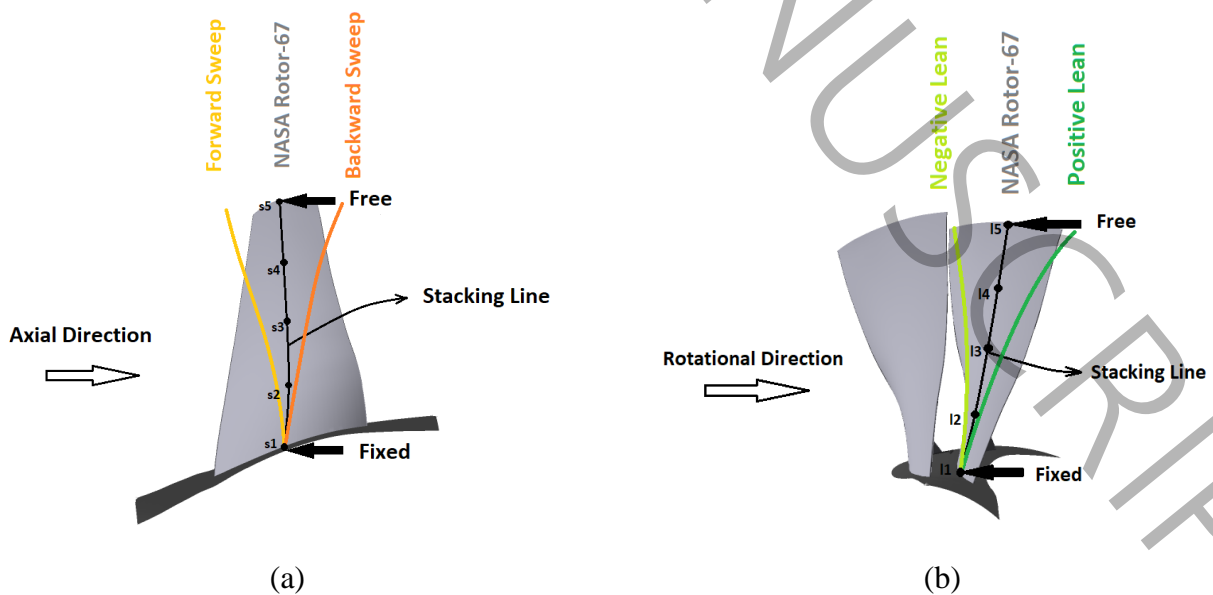
(b)

Fig. 7: Radial profile validation of performance parameters at near peak efficiency flow for (a) pressure ratio, (b) temperature ratio

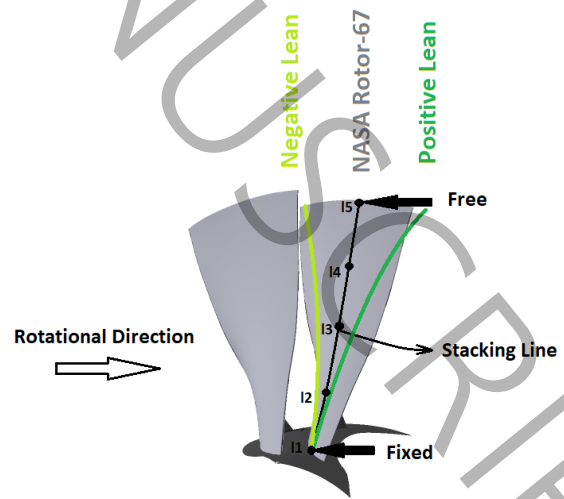
3- Optimization of axial compressor

3-1- Design variables

The compressor parametrization have changed using lean and sweep as depicted in Fig. 8. The axial-displacement of blade sections have defined as sweep [10], while the circumferential-direction of blade sections movement has define as lean [10].



(a)



(b)

Fig. 8: Rotor parameterization for (a) sweep and (b) lean blades with 5 control points

The spline algorithm has been used to parameterize new blade geometry. Five points were considered to design variables for each lean and sweep method. These five points each have upper and lower bounds that, by passing the curve through them, the stack line is generated.

To eliminate the stress concentration at the blade root, the first control point of the spline algorithm has a small range of changes. This small range between the upper and lower bounds of the first variable makes the stack line perpendicular to the hub surface.

3-1- Constraints

If the curvature of the stacking line changes several times, the blade will be encountered with high-stress concentrations. The number of curvature changes is limited to one as a constraint to avoid this issue. Therefore, for each of the lean and sweep splines, the second derivative is calculated and the number of its sign changes is counted (Eqs. (1) and (2)).

$$n_{lean} = \frac{d^2lean}{ds^2} \leq 1 \quad (1)$$

$$n_{sweep} = \frac{d^2sweep}{ds^2} \leq 1 \quad (2)$$

Table 3 indicates the upper and lower bounds of spline algorithm control points for lean and sweep. The new stacking line and three-dimensional geometry are created using the spline algorithm's coefficients.

Table 3: Coefficients bounds for leaned and swept blade

	Lean					Sweep				
Bound	l ₁	l ₂	l ₃	l ₄	l ₅	s ₁	s ₂	s ₃	s ₄	s ₅
Lower	-0.05	-2	-2	-2	-2	-0.05	-2	-2	-2	-2
Upper	+0.05	+2	+2	+2	+2	+0.05	+2	+2	+2	+2

3-2- Objective functions

The objective functions for the optimization of the rotor blade are to select the performance parameters of the compressor (mass flow rate (\dot{m}) the isentropic efficiency (η), and the total pressure ratio (PR)) at its design point. It is used the Eqs. (3) and (4) for the isentropic efficiency and the pressure ratio.

$$\eta = \frac{\left(\frac{P_{0out}}{P_{0in}}\right)^{\frac{k-1}{k}} - 1}{\frac{T_{0out}}{T_{0in}} - 1} \quad (3)$$

$$PR = \frac{P_{0out}}{P_{0in}} \quad (4)$$

3-3- Optimization methodology

Neural network coupling with optimization tools is a common method to improve turbo-machine performance that has been mentioned in the research of Heidarian et al for the squealer-tip of an axial compressor [1], Tasharofi et al [14] for double-splitter centrifugal compressor, Ekradi et al. [15] for centrifugal compressor, and Kamari et al. for airfoil [16]. The most important advantage of this optimization coupling is the reduction of the computational costs of generation in the optimization algorithm. So, the optimization procedure (including genetic algorithm coupled to the artificial neural network) is the powerful tool to search for the optimal coefficients of desired data.

3-3-1- Artificial neural network

The generated database consisting of 80 feasible cases is used. The CFD have solved to extract the compressor performance data. With using this database, three artificial neural networks have trained. These artificial neural networks (ANNs) are trained using the database to predict the objective functions.

The ANNs consist of hidden layers; each layer involves neurons. Also, the process of the training convergence of artificial neural networks is illustrated in Fig. 9. The details of ANN settings are given in Table 4. The verification of ANNs with the CFD results of the database is done and presented in Fig. 10.

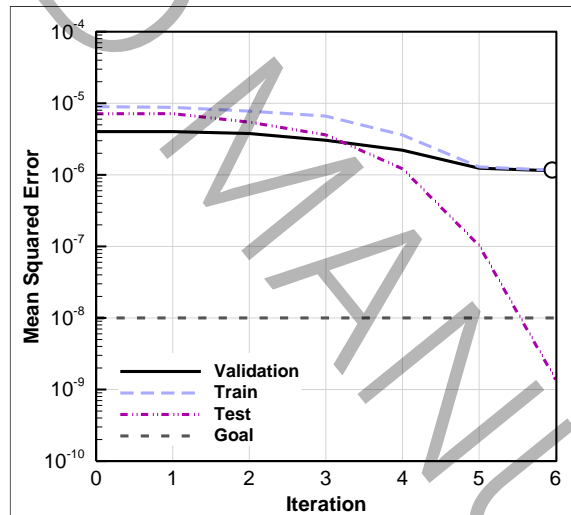


Fig. 9: Training convergence of ANN

Table 4: Details of the Artificial Neural Networks

Criteria	Function/ Value
Number of hidden layers	3
Number of neurons	6
Feeding method	Backpropagation
Number of epochs	200
Convergence goal	1e-8
Output function	Liner function
Neuron activation function	sigmoid
Data division	Random

Training algorithm	Levenberg-Marquardt
Performance	Mean squared error

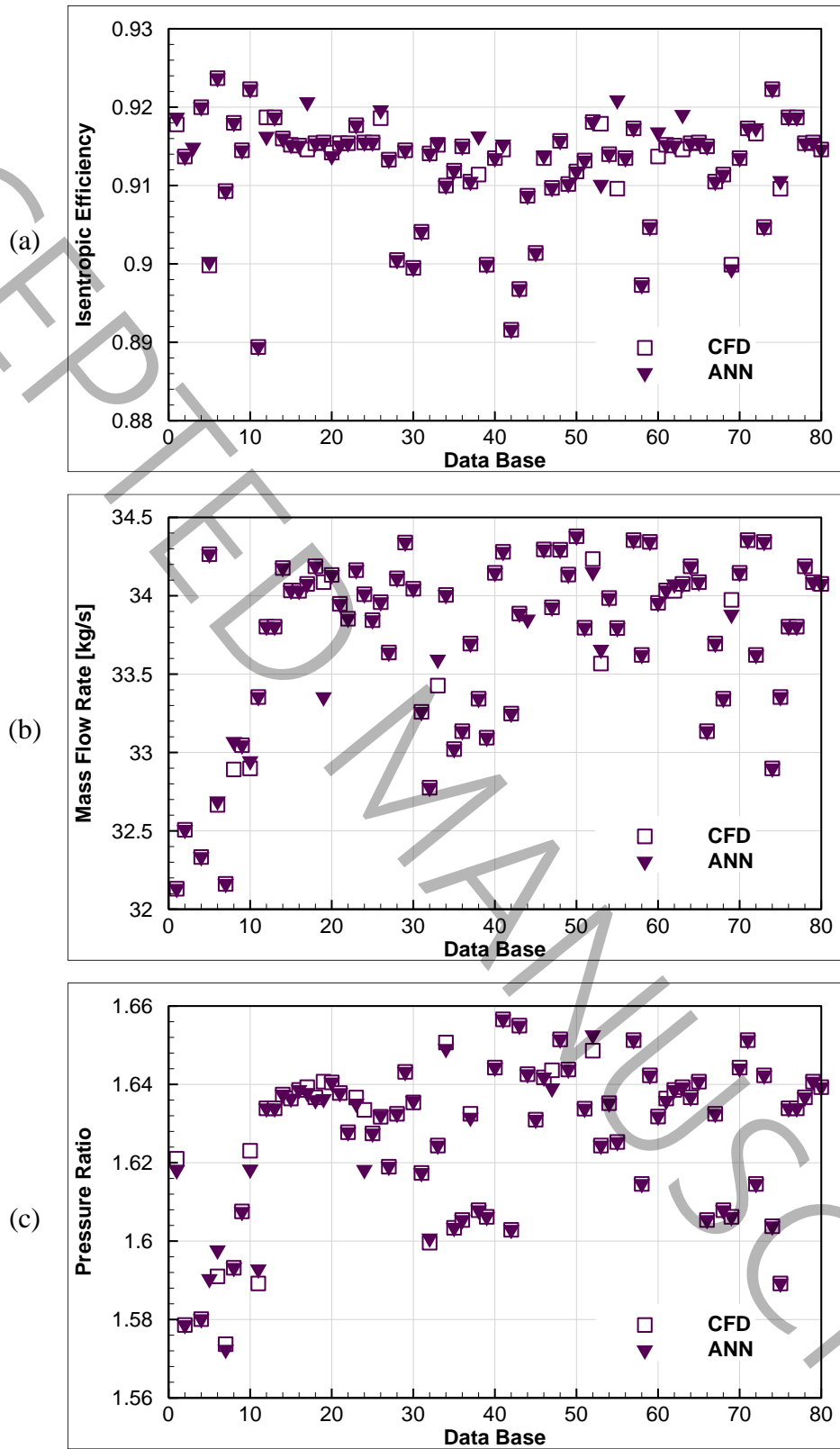


Fig. 10: Verification of Artificial Neural Network with CFD results for (a) isentropic efficiency, (b) mass flow rate, and (c) pressure ratio

In Fig. 10, the generated databases and predicted results from neural networks are simultaneously plotted for benchmarking accuracy. As inferred, minor differences in the initial data results are

observed, which practically converge to zero with increased database data, providing a very suitable validation tool as a practical instrument in the mathematical optimization of compressors.

3-3-2- Genetic algorithm

Now, the Genetic algorithm is used to find the optimum of the objective function. In the optimization loop, the ANNs predict the objective functions. For the optimum point, the flow domain is solved by CFD and validate with the ANNs. with the specified tolerance mentioned in Table 5, until the convergence criterion of optimization loop has satisfied. In all over this process, the CFD result are added to the database and the ANNs can predict better than the last result. The optimization flowchart is presented in Fig. 11, and settings are given in Table 5.

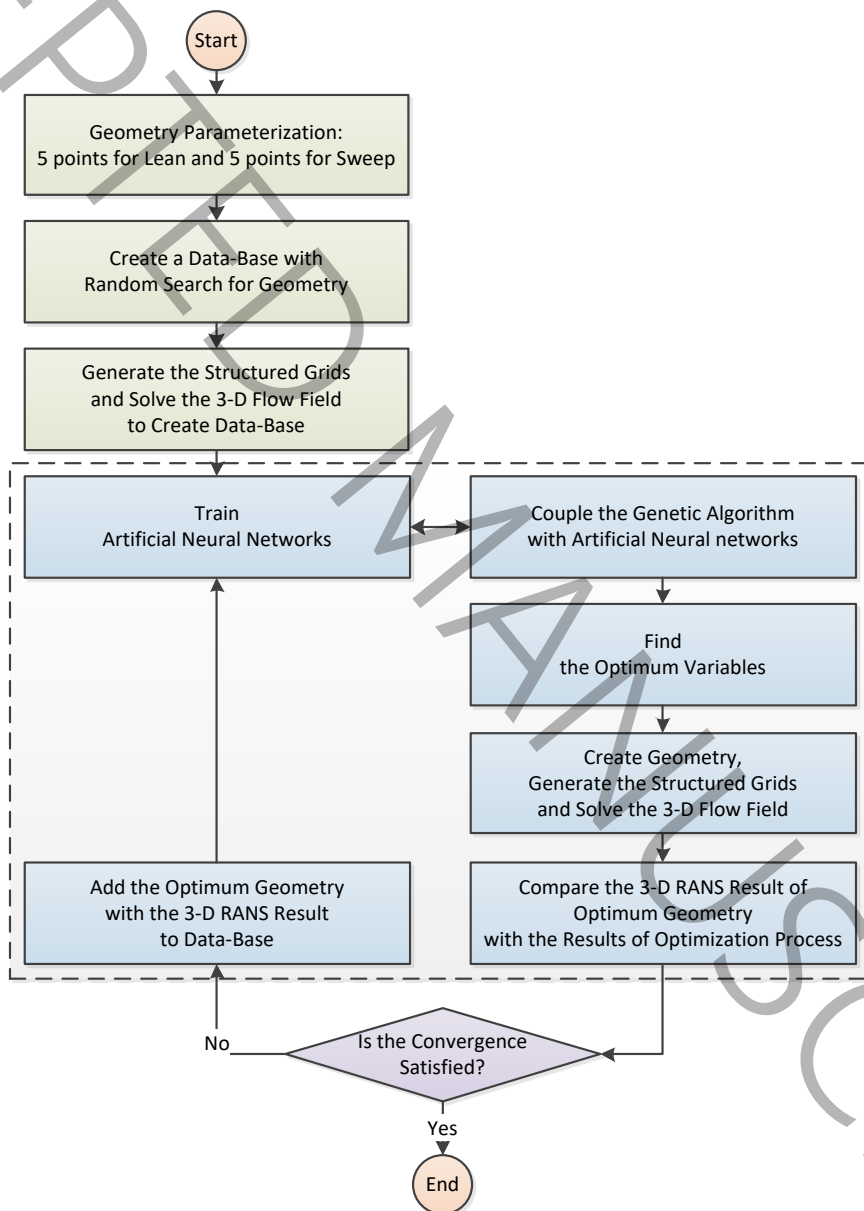


Fig. 11: Optimization procedure flowchart

Table 5: Details of the Genetic Algorithm

Criteria	Function / Value
Population Size Data	20

Generations Number	100
Convergence Criteria	1e-6
Mutation	Uniform (0.1)
Selection	Uniform
Crossover	Two-point Crossover
Fitness Scaling	Rank

3-3-3- Fitness function and penalty

The genetic algorithm finds the minimum of the objective function in the first problem to increase the compressor efficiency, mass flow rate, and pressure ratio; the objective function is defined as Eq.(5).

$$Obj = (-PR) + (-\eta) + \left(-\frac{\dot{m}}{\dot{m}_D}\right) \quad (5)$$

Some parameters may increase while the targeted efficiency may be decreased. Because the objective functions may conflict with each other. To isentropic efficiency is defined as the objective function to handle this issue. The penalty function Eq.(6) and objective function Eq.(7) are defined.

$$Penalty = \max(0, (\eta_D - \eta)) \quad (6)$$

$$Obj = (-PR) + \left(-\frac{\dot{m}}{\dot{m}_D}\right) + (10^3 \times Penalty) \quad (7)$$

3-4- Feasible bounds

The results of the increase (or decrease) in objective functions of shape-changing compressors with simultaneous lean and sweep modifications have been evaluated and depicted in Fig. 12.

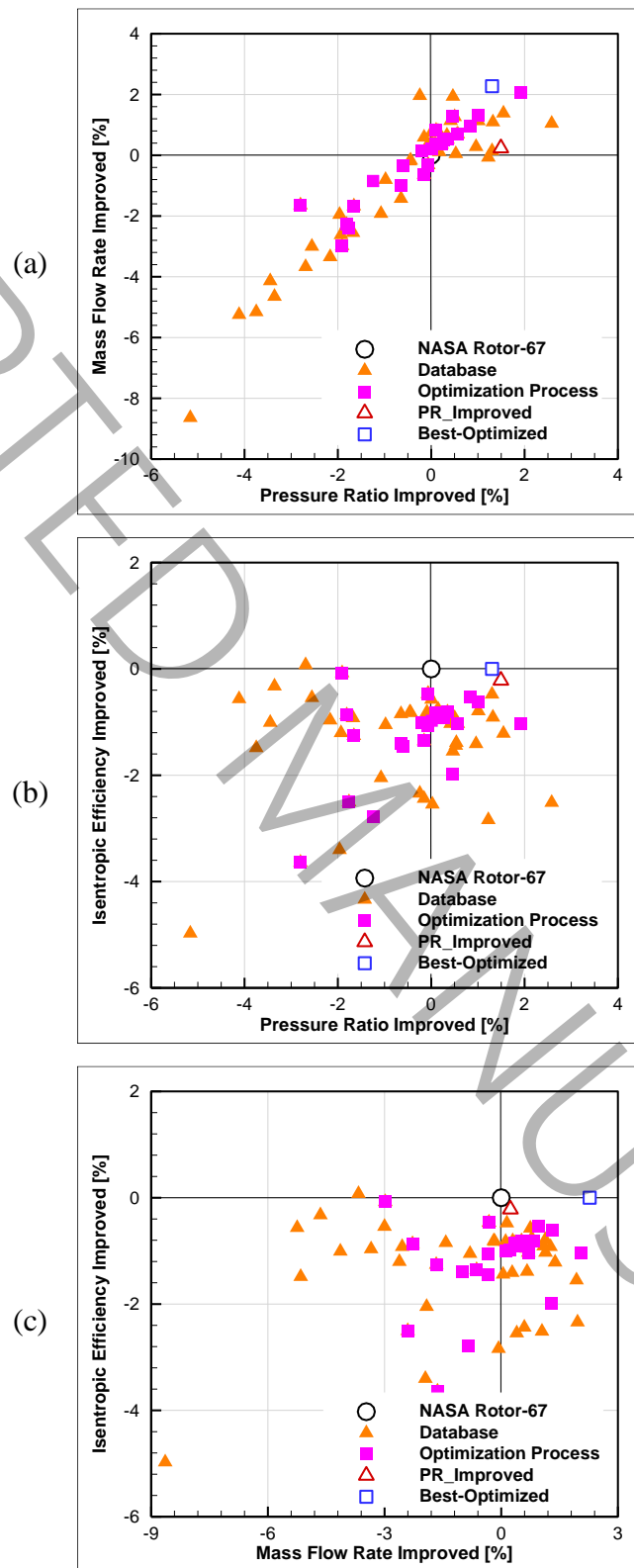


Fig. 12: Comparison of the improvement of optimized rotor and NASA Rotor-67 for (a) pressure ratio-mass flow rate, (b) pressure ratio-isentropic efficiency and (c) mass flow rate-isentropic efficiency

According to the figure, the initial databases and optimized geometries extracted in the genetic algorithm process are illustrated, indicating the flexible areas for performance changes in compressors. The two superior geometries selected based on optimization process constraints, named PR-Improved and Best-Optimized, have maintained the previous isentropic efficiency while maximizing the increase in pressure ratio and mass flow rate. These two geometries are detailed and explained in the results.

4- Result and discussion

The results of three-dimensional analysis of axial compressor flow and optimized rotors have been processed, leading to improvements in the design point results. It is worth mentioning that the improvements are not only evident at the design point but also show relative enhancements in other off-design conditions, highlighting the utilization of these characteristic curves in the thermodynamic cycle modeling.

4-1- Characteristic maps

After reaching the optimized rotors that demonstrated compatibility with the imposed constraints and showed relative improvements at their design point, the characteristic curves of their design speed have been completed and compared with each other in Fig. 13.

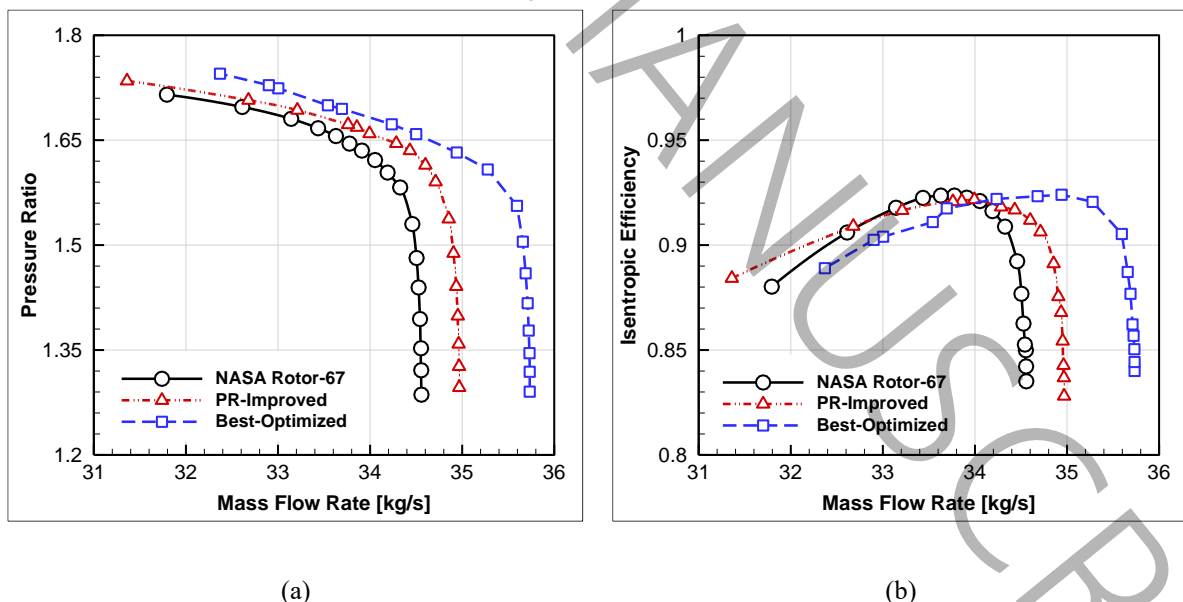


Fig. 13: Comparison of the optimized rotor and NASA Rotor-67 for (a) pressure ratio-mass flow rate and (b) isentropic efficiency-mass flow rate

The results indicate that both geometries of the optimized rotors have shown improvements in mass flow rate at the design point and other points close to the stall regions. In the best rotor, the improvement in performance efficiency compared to the base geometry has been striking, and these values are presented in the Table 6.

Table 6: Performance parameters and its improvement for the optimized rotor at design, choke and stall point

point	Case	Performance parameters			% Improved objective functions		
		Pressure ratio	Isentropic efficiency	Mass flow rate [kg/s]	Pressure ratio	Isentropic Efficiency	Mass flow rate
Choke	Rotor-67	1.286	0.835	34.558	---	---	---
	PR-Improved	1.296	0.828	34.968	0.801	-0.843	1.188
	Best-Optimized	1.291	0.840	35.733	0.334	0.589	3.403
Design	Rotor-67	1.635	0.923	33.91	---	---	---
	PR-Improved	1.6594	0.921	33.99	1.486	-0.098	0.245
	Best-Optimized	1.6563	0.923	34.681	1.297	0.174	2.020
Near-stall	Rotor-67	1.715	0.880	31.793	---	---	---
	PR-Improved	1.735	0.884	31.360	1.149	0.454	-1.362
	Best-Optimized	1.745	0.889	32.370	1.746	1.000	1.815

The pressure ratios of the PR-Improved and Best-Optimized rotors have improved by 1.486 % and 1.297 %, respectively. The isentropic efficiency of the PR-Improved decreased by only 0.1%. By adding a penalty and re-optimization, the optimal rotor with a relative improvement of 0.17% efficiency is obtained.

The Best-Optimized rotor has the most significant increase in mass flow at the design point, 2.020 %. The choking mass flow of the optimal geometries has also improved as well as its design point, which is another inferred result of the characteristic curve. This improvement in choking mass flow of the Best-Optimized rotor is 3.403% compared to the Rotor-67.

4-2- Surge margin

As the objective functions are improved at the design point, the surge margin can also be calculated to evaluate the improvement in the optimal geometry relative to the reference geometry. Eq.(8) is presented to calculate the surge margin [17].

$$SurgeMargin = 1 - \left(\frac{PR_D}{PR_{NS}} \right) \times \left(\frac{\dot{m}_{NS}}{\dot{m}_D} \right) \quad (8)$$

The surge margin and its enhancement percentage are calculated and presented in Table 7.

Table 7: Surge Margin and its improvement for the optimized rotors

Surge Margin

Case	Surge Margin	Improved [%]
Rotor-67	0.106	---
PR-Improved	0.118	10.727
Best-Optimized	0.112	5.128

The research study [1] [14] shows that a positive sweep has more surge margin than a negative sweep. In this study, the surge margin enhancement for first and second optimal compressors equals 10.7% and 5.1 %.

4-3- Radial profile

Comparison of hub-to-tip distribution of pressure ratio and isentropic efficiency parameters in optimized rotors relative to the Rotor-67, extracted with the help of circumferentially averaged mass distribution, is presented in the Fig. 14.

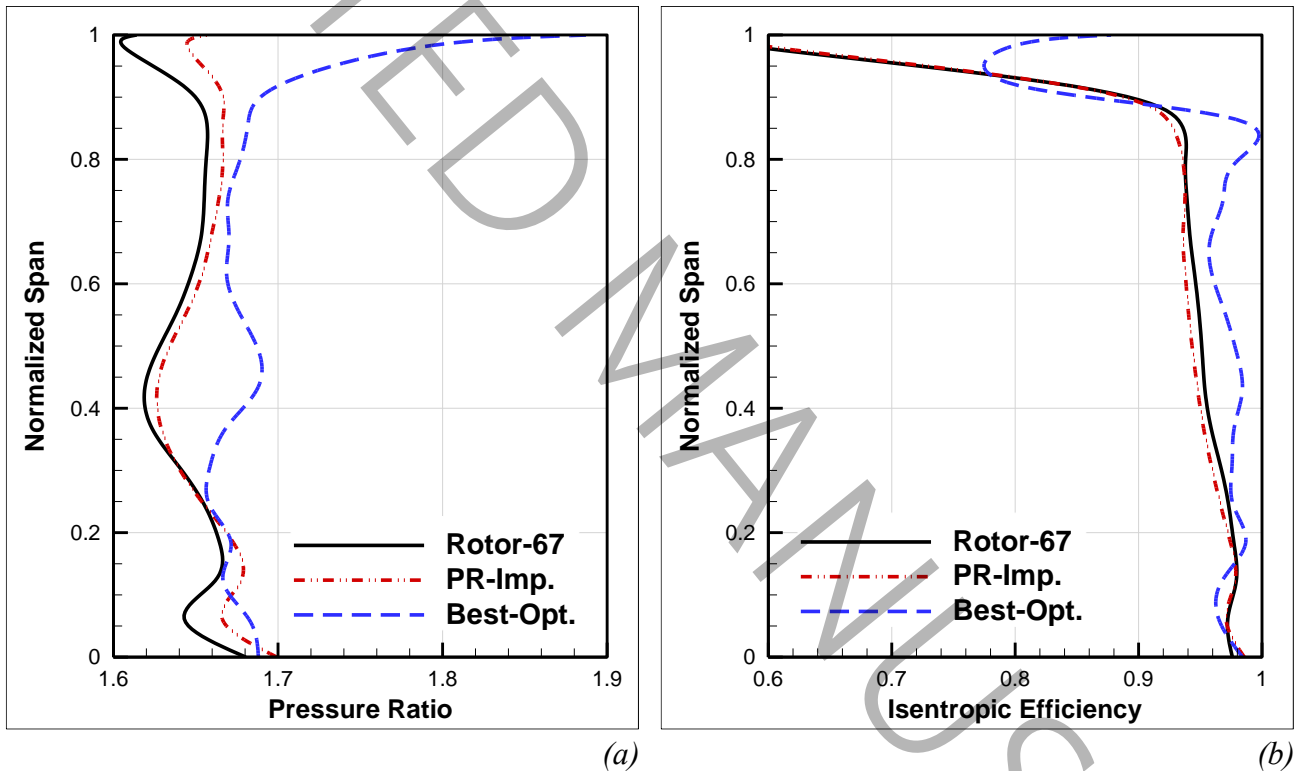


Fig. 14: Comparison of the radial distribution of optimized rotor and NASA Rotor-67 for (a) pressure ratio and (b) isentropic efficiency

According to these results, improvements in isentropic efficiency performance are clearly observed in near-design tip speeds (above 80% span), especially in the geometry of the best rotor which has been swept downstream in the downstream direction of the flow.

The noticeable difference seen for the pressure ratio and isentropic efficiency ratio for Best-Optimized compared to tip region geometry is due to the backward sweep that was obtained in extracting superior rotor based on AI model, resulting in higher performance.

4-4- Pressure loading effects

4-4-1- Streamline distribution and shock wave

The distribution of pressure ratio of optimized rotors compared to the baseline geometry, in two pressure and suction sides, for comparison, is illustrated in Fig. 15 (Rotor-67 with grey, PR-Improved with red and Best-Optimized with blue colors)

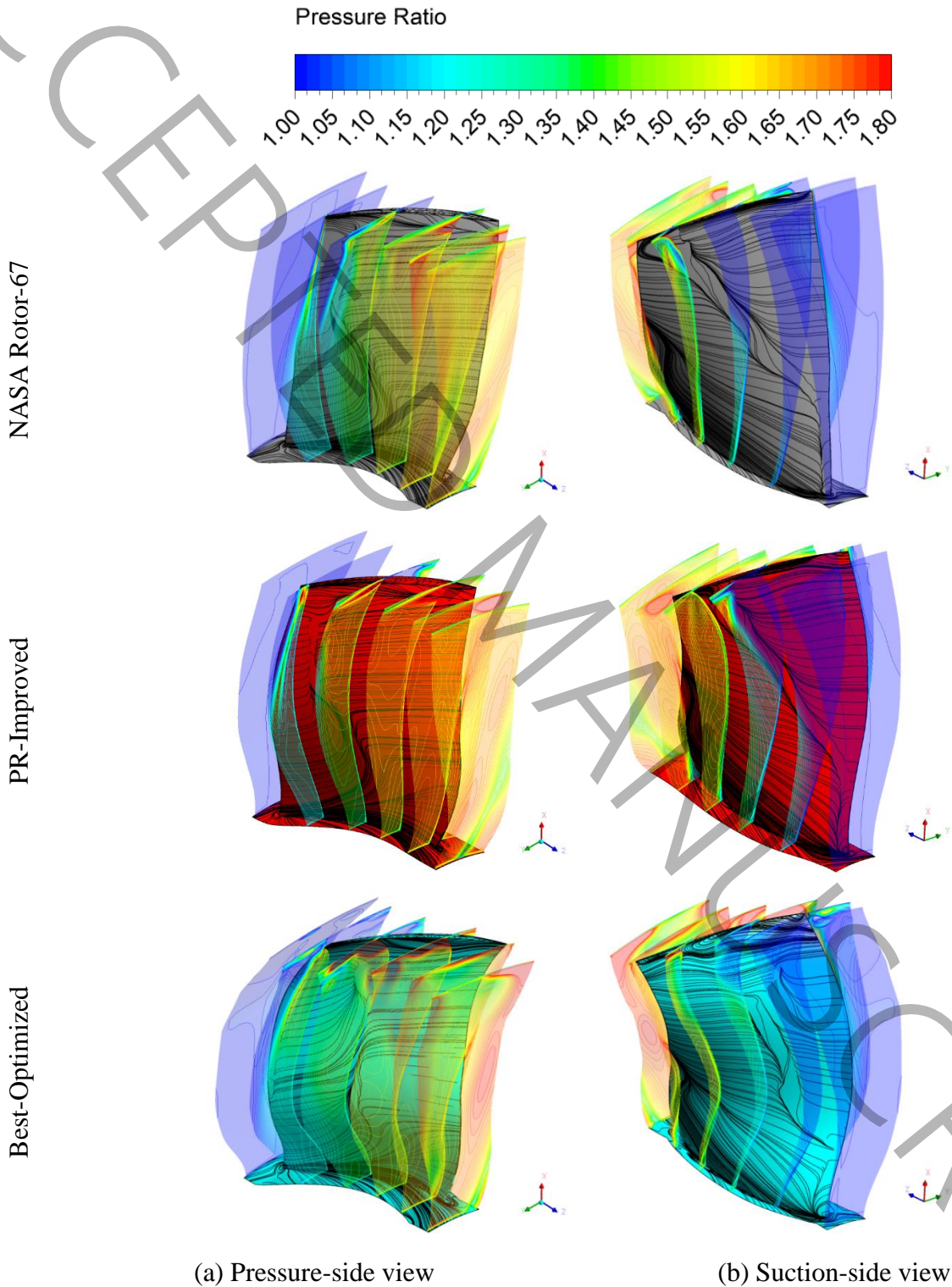


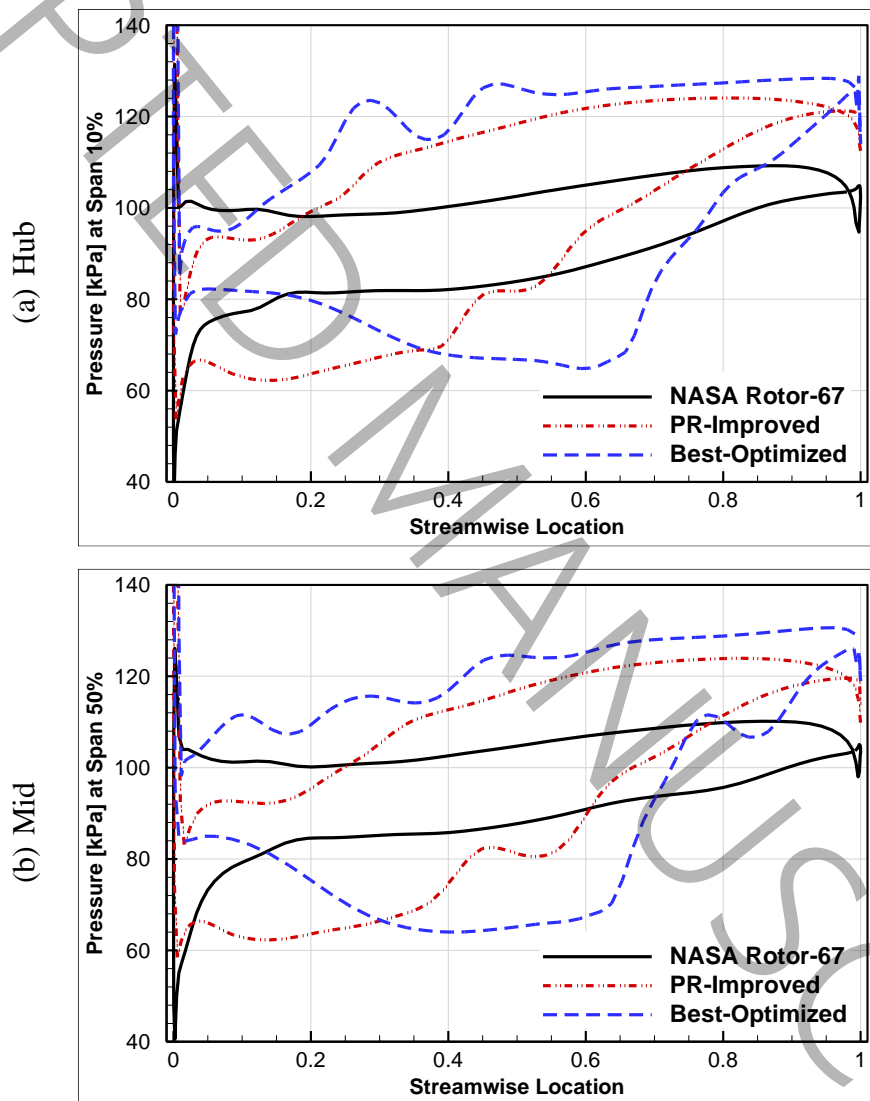
Fig. 15: Comparison of pressure contour at (a) pressure-side and (b) suction-side for: NASA Rotor-67, PR-Improved rotor and Best-Optimized rotor

According to the contour results, the location of the normal shock wave occurrence in the baseline rotor has been converted to a more inclined shock in the optimized rotors. Therefore, as expected, lower pressure drop and higher pressure loading can be achieved in the optimized rotors, leading to optimal compressor performance.

As apparent, the spatial shape of the shock is influenced by the blade curvature [8]. So, the pattern of the blade streamline at the normal shock locations (as mentioned) causes the flow separation. However, this occurrence is directed downstream in the optimal rotors, and therefore it has reduced the flow separation and improved the compressor's performance.

4-4-2- Blade pressure loading

The pressure surface distribution of the optimal rotor surfaces is also extracted and calculated compared to the baseline rotor and presented in Fig. 16 from the leading edge to the trailing edge.



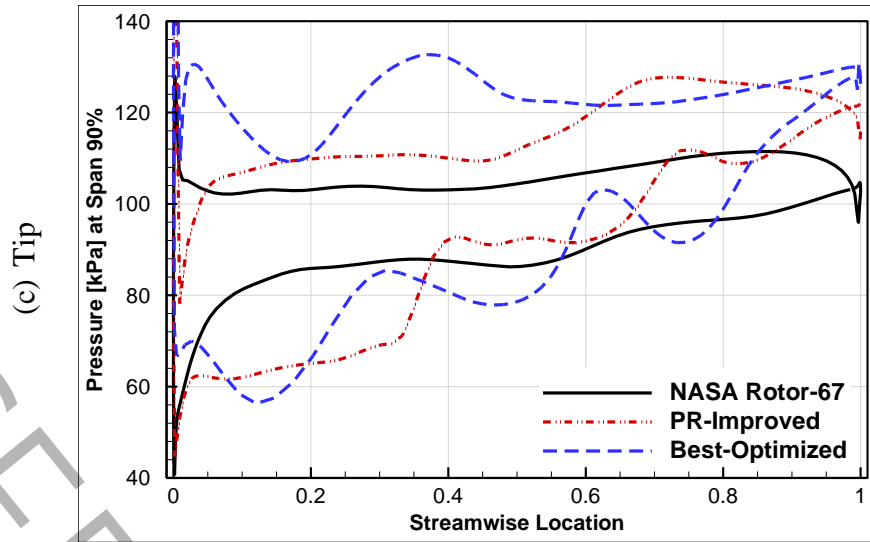


Fig. 16: Comparison of the pressure distribution of optimized rotor at the (a) hub, (b) mid and (c) tip spans

Thus, improving compressor performance can be achieved by displacing the normal shock to inclined shock, which is due to the direct effects of backward sweep three-dimensional compressor geometry.

Furthermore, the pressure loading of Best-Optimized rotor, although seen to be higher than two other rotors in its pressure surface, has experienced delayed flow separation on its suction surface, leading to better performance on the performance curve.

4-5- Mach number distribution

Fig. 17 displays the distribution of relative Mach number along the streamwise of the optimized rotors compared to Rotor-67 in a contour graphic form.

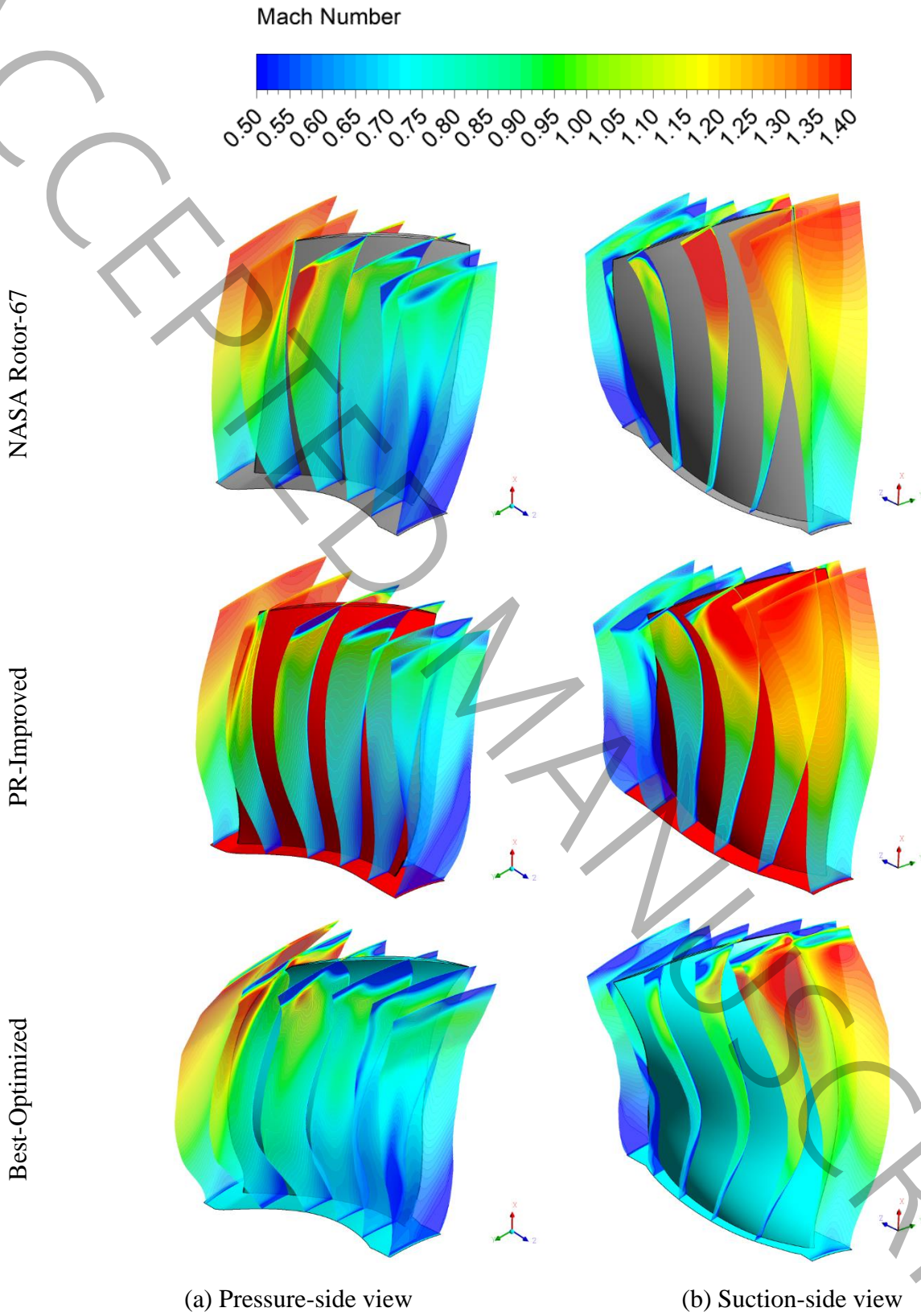


Fig. 17: Comparison of pressure contour at (a) pressure-side and (b) suction-side for: NASA Rotor-67, PR-Improved rotor and Best-Optimized rotor

Attention to the distribution of Mach number along the entire flow path (from leading edge to trailing edge) suggests that loading resulting from simultaneous changes in lean and sweep has had more uniform effects on the distribution of relative Mach number along the flow path. Although relative Mach numbers close to the magnitude of 1.4 have been maintained near the tip region, it seems that in optimal rotors, the difference between the minimum and maximum values of these distributions is less visible. This issue has also been discussed and evaluated in blade-to-blade section.

4-6- Meridional-view Effects

Fig. 18 shows the distribution of meridional velocity for the two optimized rotors compared to Rotor-67. This velocity can be an indicator of uniformity and magnitude of speed in the aerodynamic field of the new rotors.

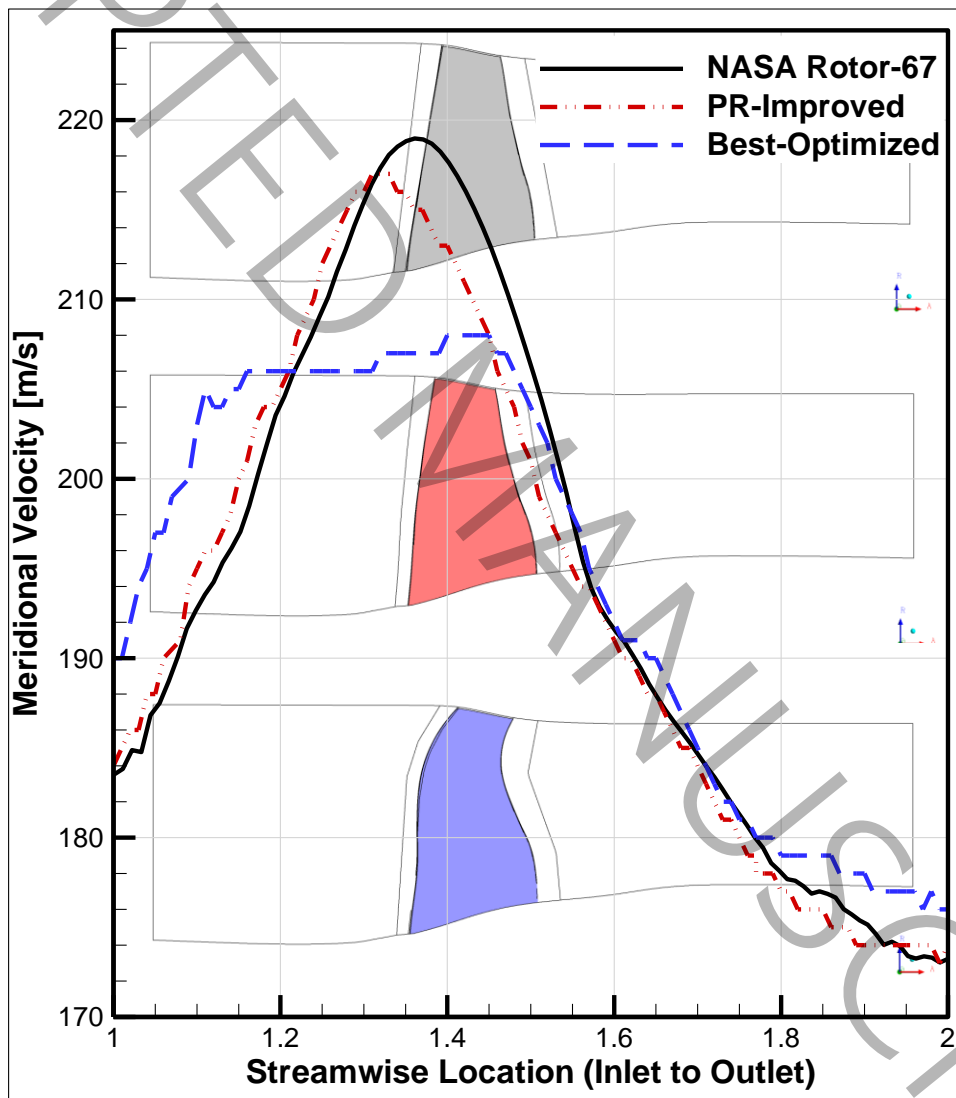


Fig. 18: Comparison of meridional velocity of optimized rotors with NASA Rotor-67

In the blade pressure loading section, it was observed that the two optimized rotors had higher pressure performance compared to Rotor-67, indicating a more uniform axial velocity distribution, covering a larger space of the streamwise aerodynamic field from hub to shroud. Therefore, the accuracy of this more uniform axial velocity distribution compared to Rotor-67 can be achieved as shown in Fig. 18.

4-7- **Blade-to-Blade Effects**

The effects of lean and sweep can be investigated in altering the relative Mach contour and improving the incidence and deviation angles of in three sections: hub, mid, and shroud. This is because changing the airfoil arrangement leads to changes in loading and displacement of these quantities, which can lead to improvements.

Fig. 19 shows the relative Mach contour comparison of designed points of Rotor-67 and the optimal rotors for three sections hub, middle, and shroud.

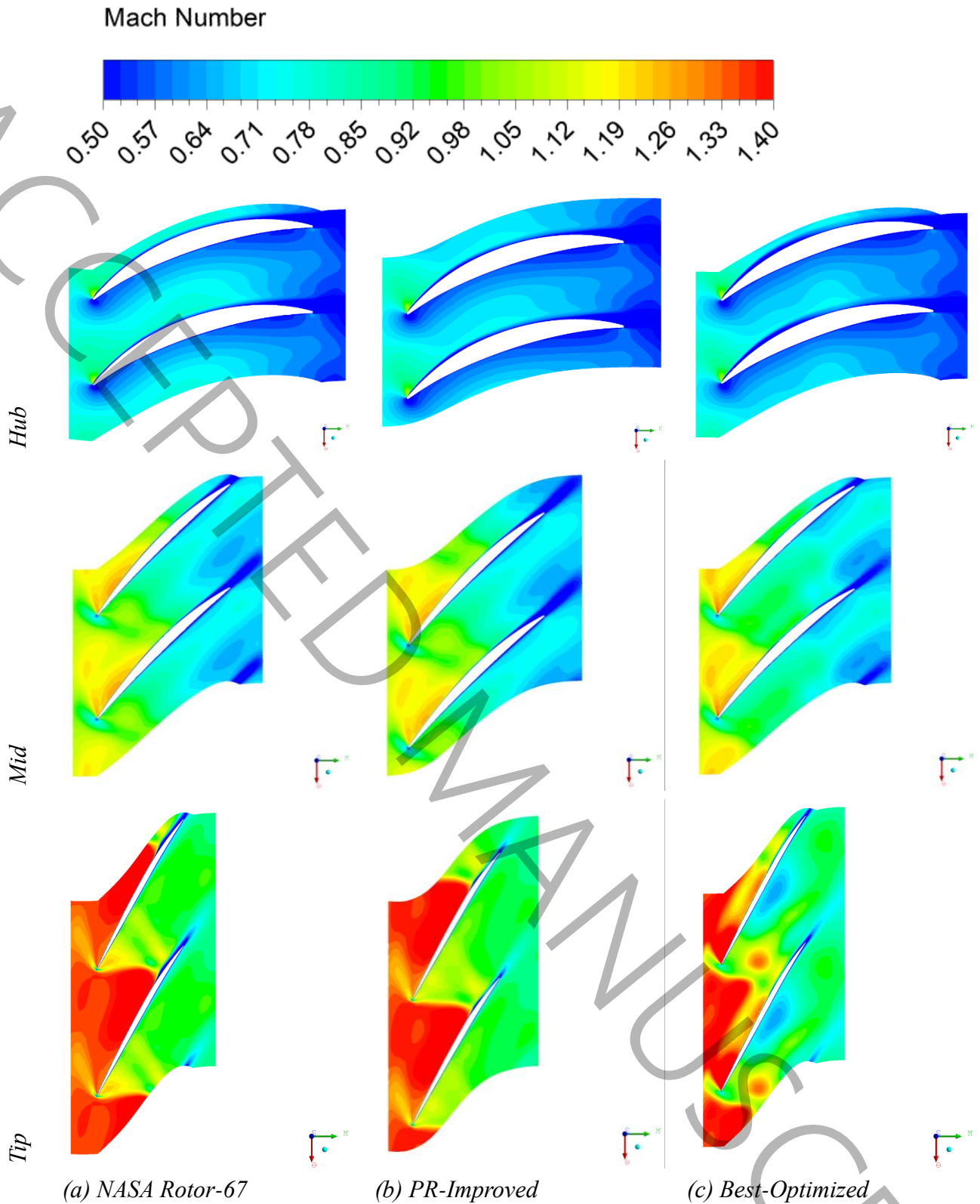


Fig. 19: Comparison of relative Mach number for:
(a) NASA Rotor-67, (b) PR-Improved rotor and (c) Best-Optimized rotor

The blade tip contour shows that the maximum Mach number (1.4) covers a larger area of the flow path between the two blades of the second optimal geometry; the shock profile is delayed, and therefore, a higher performance of the compressor is obtained at its design point. The mass flow of this compressor has also reached its maximum in comparison with the other two ones.

4-8- Circumferential Effects

The applied changes in the optimal rotors lead to circumferentially aerodynamic effects, which in this section are discussed in terms of velocity curl of optimized rotors compared to the baseline design.

4-8-1- Velocity Curl

The distribution of normalized circumferential velocity gradient in the tip region of the rotor blade is extracted just behind the rotor and presented in the Fig. 20. These curls, which depict a measure of instability, are less in the optimal rotors at the optimum point compared to the baseline geometry.

The normalized velocity curl that were previously observed in the side wall of the tip region in Rotor-67 have shown a considerable decrease with changes in the circumferential direction, which can be an indicator of increased orderliness in the streamlines of the critical tip region. Its effects on the flow smoothness, increased performance range, and enhanced stability at the blade tip margin are clearly evident.

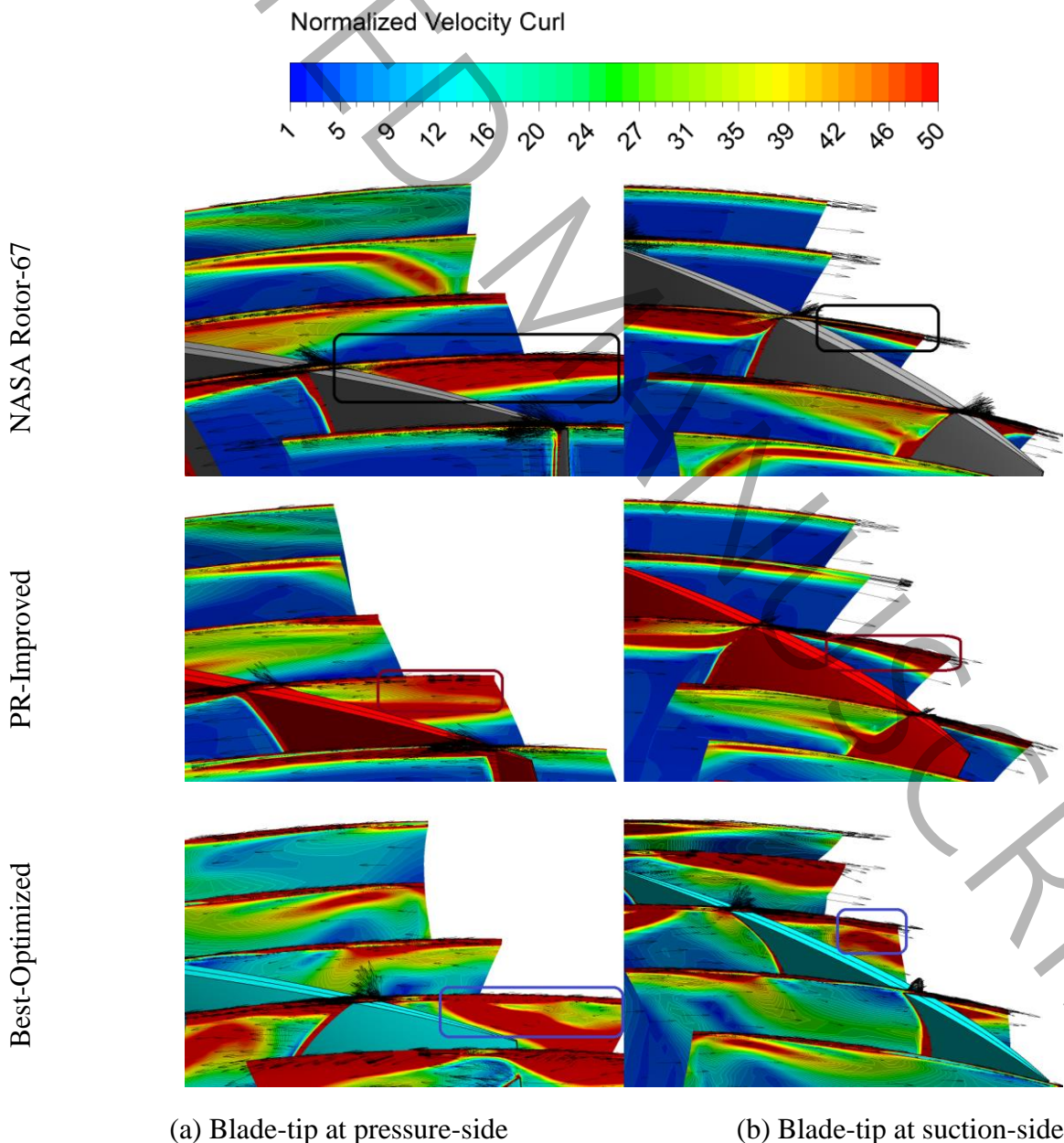


Fig. 20: Comparison of normalized velocity curl contour at blade-tip of (a) pressure-side and (b) suction-side for: NASA Rotor-67, PR-Improved rotor and Best-Optimized rotor

4-8-2- Entropy Generation

Fig. 21 illustrates the contour distribution of normalized entropy (per 100 [J/kg.s]) rotor outlet at the design point for two optimal geometries compared to Rotor-67.

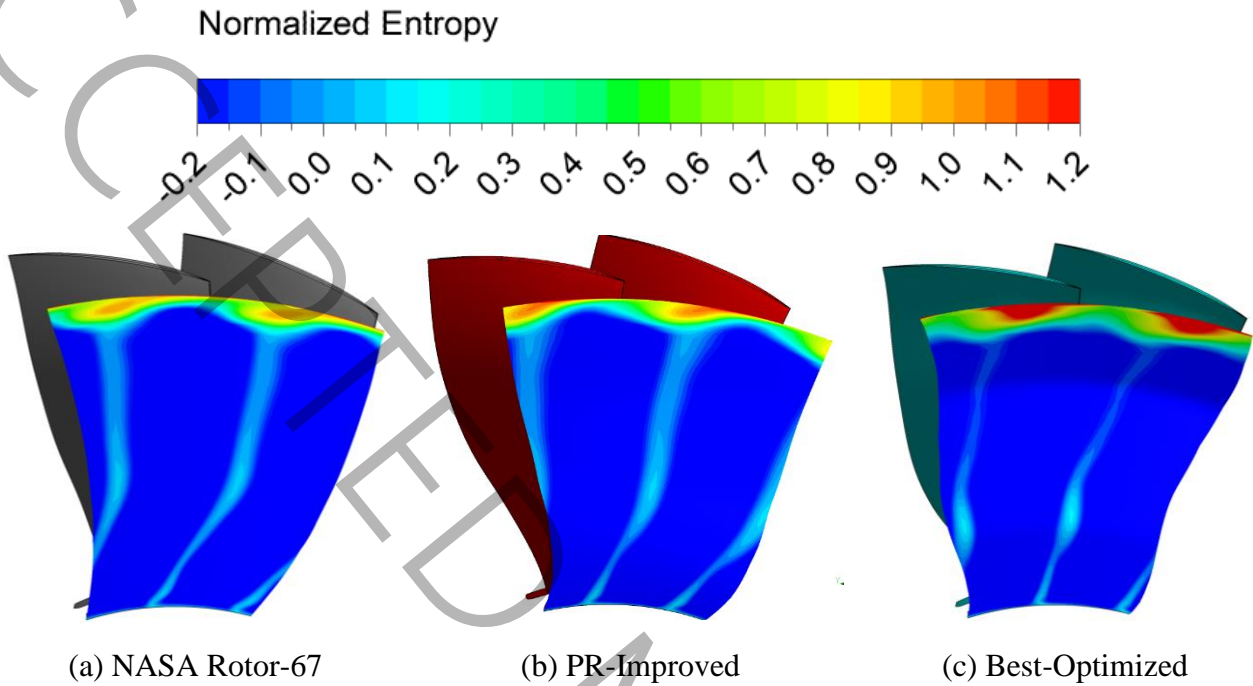


Fig. 21: Comparison of normalized velocity curl contour at blade-tip of (a) pressure-side and (b) suction-side for: NASA Rotor-67, PR-Improved rotor and Best-Optimized rotor

It is deduced from the entropy contour distribution that for two optimal geometries, between 0% to 90% span, an almost uniform distribution with little change in entropy is observed (unlike Rotor-67). However, locally, the entropy of the optimal blade tips is higher than Rotor-67, which could be due to changes in the sweep tip and a relative increase in the Mach number. Nevertheless, the overall average output surface of the compressor in optimal rotors has greater uniformity.

4-9- Geometry Comparison

The geometric changes that occurred in the optimization process for the optimized rotors compared to a baseline rotor have been illustrated in this section, including the spanwise and sweep angles of the sections depicted in the top view.

4-9-1- Stacking Line

Fig. 22 and Fig. 23 shows the changes in the lean and sweep of optimal rotors compared to the baseline rotor for 3-D and 2-D views. The optimal lean and sweep coefficients are also presented in Table 8.

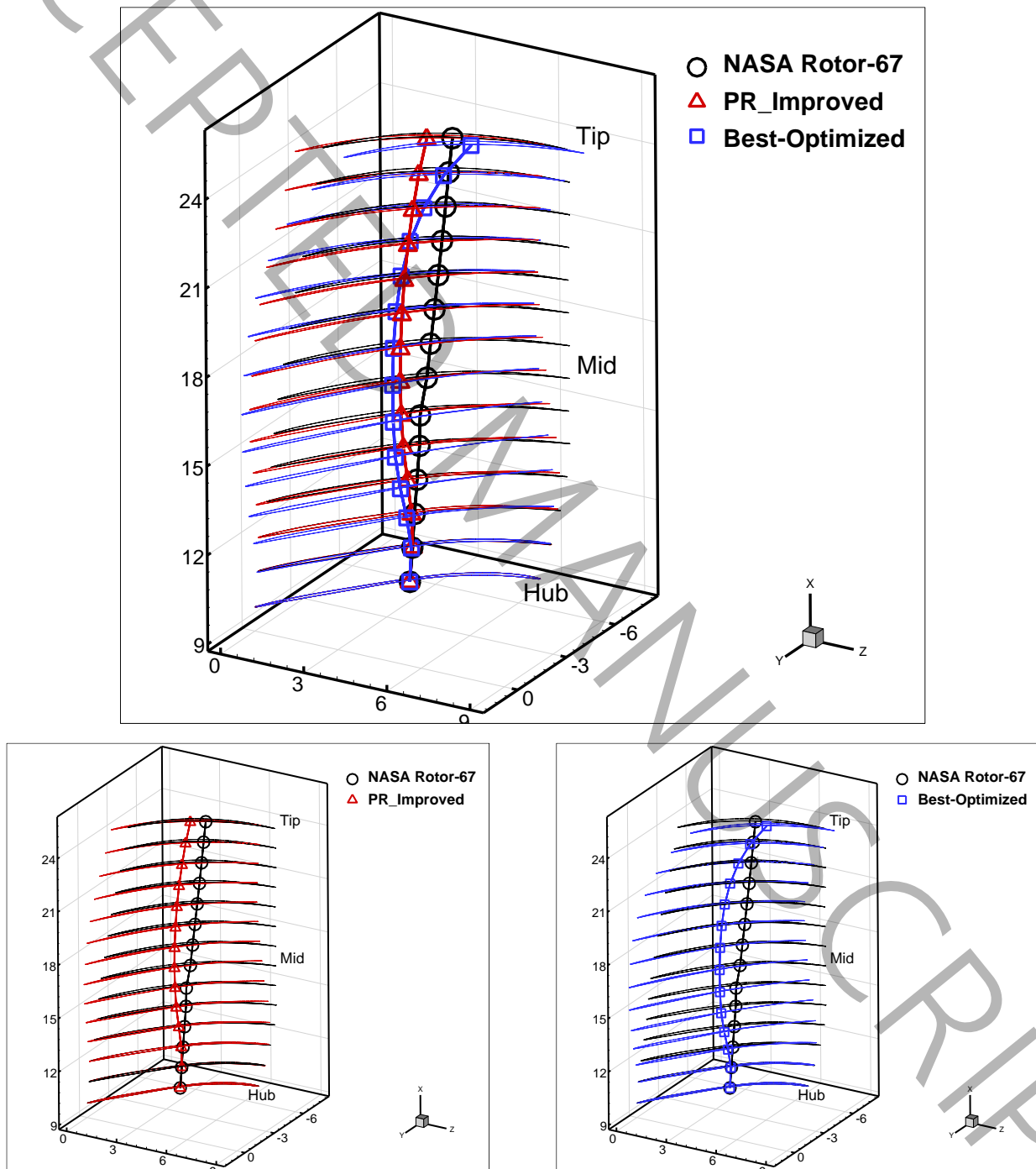
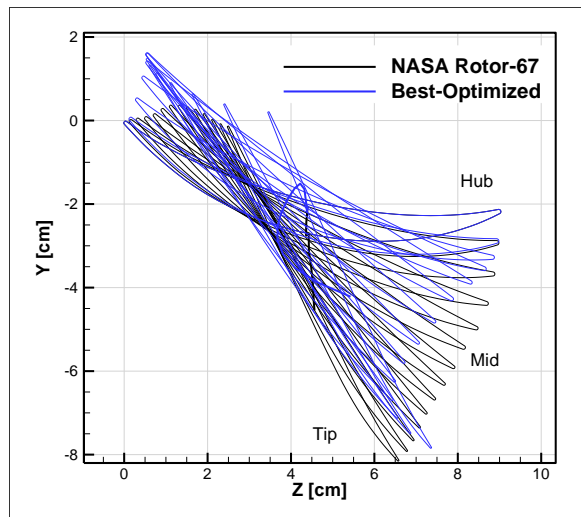
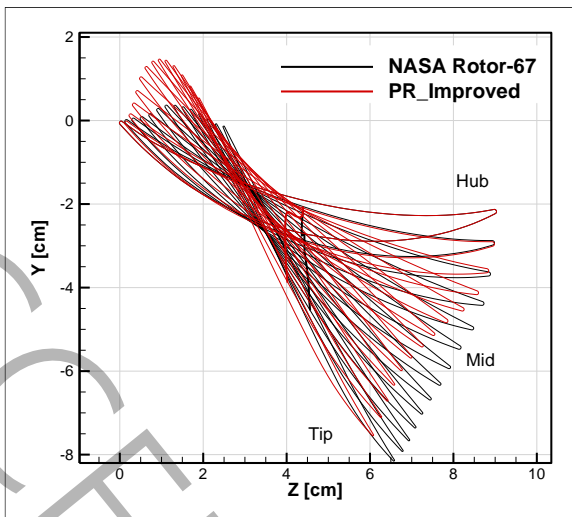
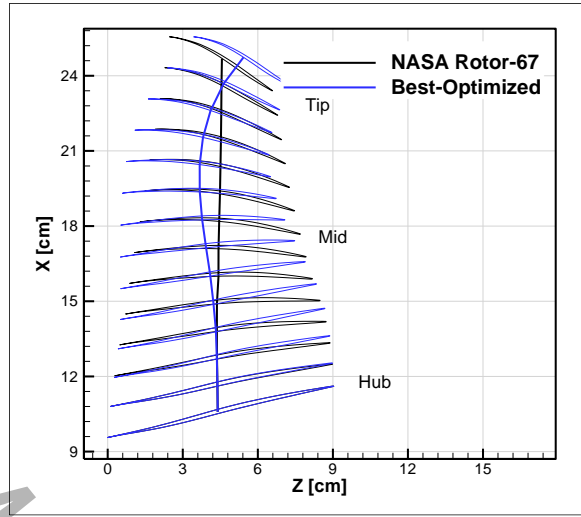
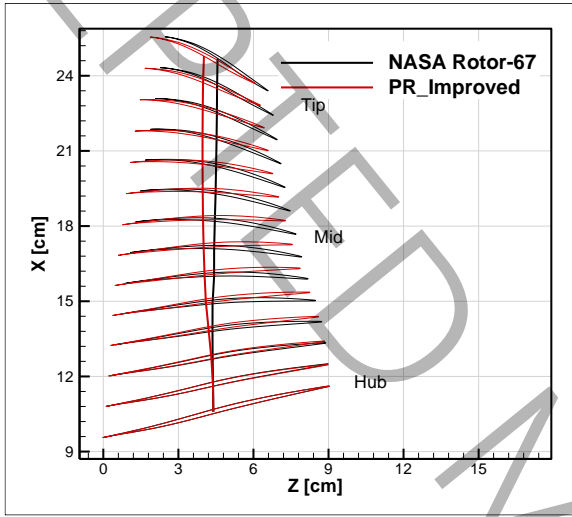


Fig. 22: Comparison of 3-D views of PR-Improved and Best-Optimized rotors with NASA Rotor-67

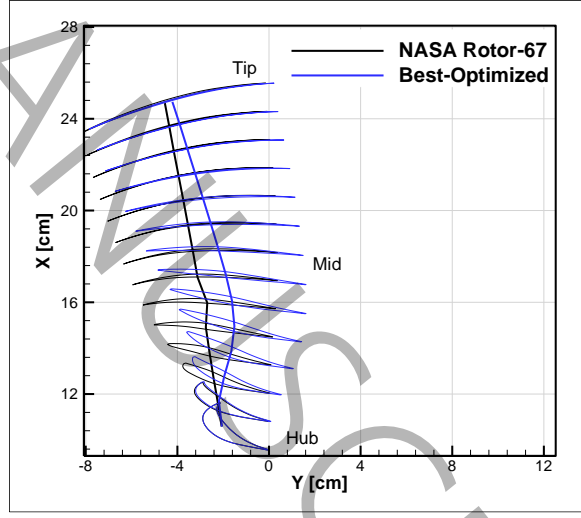
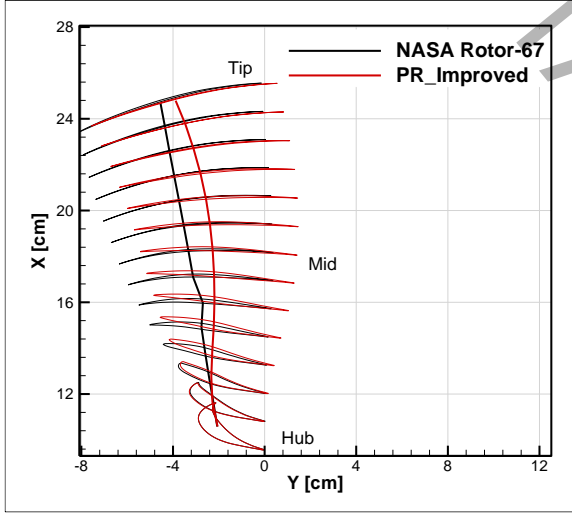
Top-View



Meridional-View



Front-View



(a)

(b)

Fig. 23: Comparison of the top, meridional and front views of (a) PR-Improved and (b) Best-Optimized rotors with NASA Rotor-67

Table 8: The lean and sweep coefficients of optimized rotors

Bound	Lean					Sweep				
	l ₁	l ₂	l ₃	l ₄	l ₅	s ₁	s ₂	s ₃	s ₄	s ₅
PR-Improved	0.048	-0.385	-1.003	-1.163	-0.671	-0.018	0.741	1.103	1.089	0.938
Best-Optimized	0.020	-1.087	-1.202	-0.775	-0.342	0.007	0.297	1.476	1.500	-1.498

As seen in Table 8, PR-Improved optimal rotor, have set a forward sweep, while the Best-Optimized rotor initially leans forward sweep and then enters into tip back sweep. This behavior trend, which leads to maximum improvement in rotor performance, has been previously observed in the Benini research.

The lean behavior of both optimal rotors was the same; with a 40% change in incidence seen for optimal rotors (Best-Optimized rotor has more curvature in the span of about 30% than the PR-Improved rotor). The tip of the optimal rotors has also returned to the optimal airfoil range.

Now, the comparison of the optimization results of the other studies carried out regarding lean and sweep axial compressors is given in Table 9. In most of these studies, adding a penalty has improved the objective functions and prevented the reduction of other objective functions.

Table 9: The brief of the lean and sweep study in comparison with present work

Study	Test Case	Pressure ratio increment	Mass Flow Rate increment	Isentropic Efficiency increment
Benini	Rotor-37	5.5 %	NA	-0.8 %
		0	NA	1.5 %
Oyama	Rotor-67	0.6 %	0.46 %	1.783 %
Samad	Rotor-37	1.62 %	NA	-0.04 %
		-1.55 %	NA	1.41 %
		1.25 %	NA	0.51 %
Wang X.D.	An industrial case	1 %	-0.04 %	1.1 %
Huang	Rotor-37	1.4 %	0.9 %	0.5 %
		0.1 %	0.2 %	1.2 %
		0	0.1 %	1.2 %
Cao	Rotor-37	0.05 %	NA	0.8 %
Present Work	Rotor-67	1.486	0.245	-0.098
		1.297	2.020	0.174

5- Engine Performance

The performance study is modeling and analyzing the thermodynamic cycle of a turbojet engine in this part. The compressor is powered by the turbine, which extracts energy from the expanding gas passing through it. The engine converts internal energy in the fuel to kinetic energy in the exhaust, producing thrust [18]. The schematic view of the engine is shown in Fig. 24.

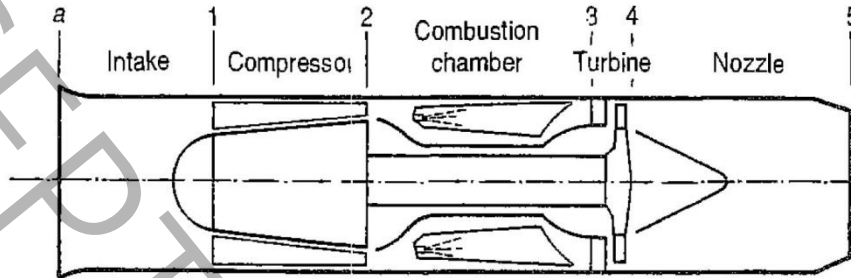


Fig. 24: a single spool turbojet engine [19]

The in-house thermodynamic code has been developed for on-design and off-design performance calculations. The engine's characteristics are used from GasTurb software [20] that is close to the present test case. For the axial compressor, the Rotor-67 is assumed the first compressor stage and the other multi-stage are modeled with a certain pressure ratio and isentropic efficiency.

In this in-house code modeling, the gaseous fluid is assumed to be composed of water (H_2O), carbon dioxide (CO_2), oxygen (O_2), nitrogen (N_2), argon (Ar), and hydrogen (H_2). Therefore, the mass fraction, molar fraction, gas constant, and specific heat at constant volume and constant pressure are calculated using the Eqs.(9), (10), (11), and (12).

$$MW_{mix} = \frac{1}{\sum_{i=1}^6 \frac{x_i}{MW_i}} \quad (9)$$

$$Y_i = x_i \times \frac{MW_{mix}}{MW_i} \quad (10)$$

$$R = \frac{R_{univ}}{MW_{mix}} \quad (11)$$

$$k = \frac{c_p}{c_v} = \frac{c_p}{c_p - R} \quad (12)$$

Once the mass fraction of each component is known, the enthalpy of the mixture is calculated by the Eqs. (13) and (14). The specific heat of constant pressure is a third-degree polynomial function of temperature, written in Eq.(15).

Component	Parameter	Unit	Value
Turbine	Isentropic Efficiency	%	89
Nozzle	Isentropic Efficiency	%	98

To evaluate the effect of compressor optimization in the design point conditions, the performance parameters of Rotor-67 and the best-optimized rotor (Best-Optimized rotor) are included in the turbojet cycle, and Thrust was subsequently calculated.

5-2- Off-design Cycle

To investigate the effect of aerodynamic optimization of the first stage of the compressor on the off-design performance, the code for solving the equations of the turbojet engine has been developed. The process of off-design cycle analysis is discussed in detail in [19]. The compatibility equations are solved by the Newton-Raphson solver, and the Thrust [18] [19] [20] are computed. Fig. 26 shows the on-design and off-design processes.

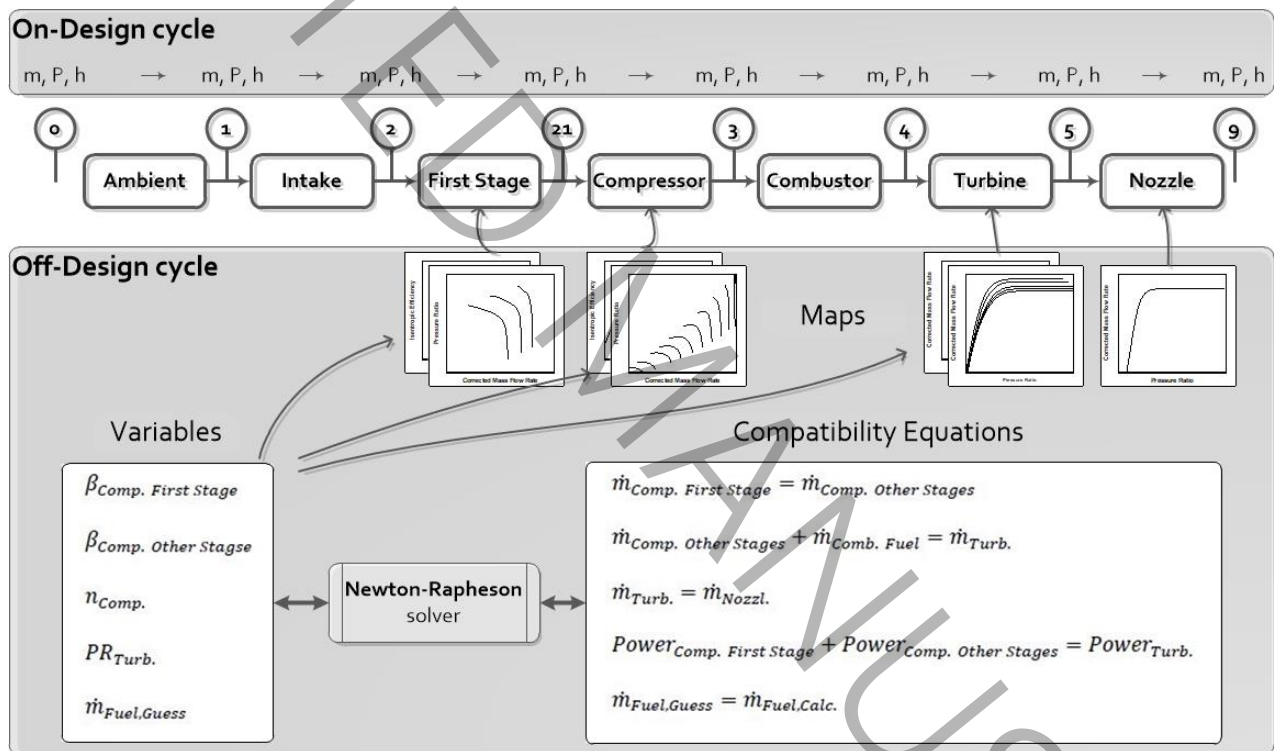
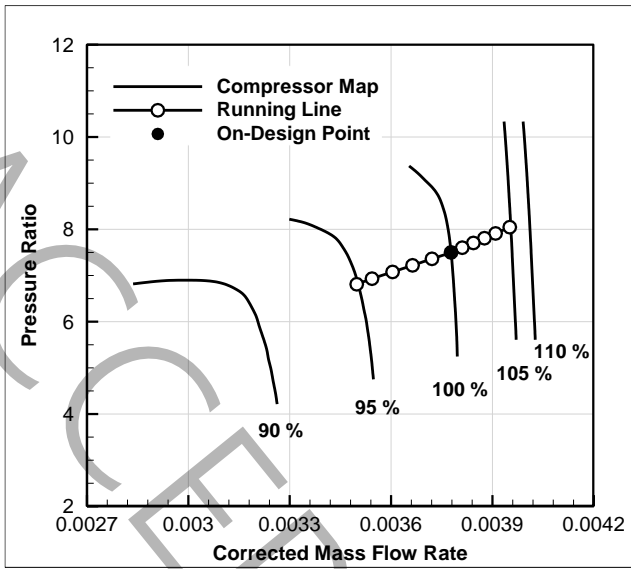
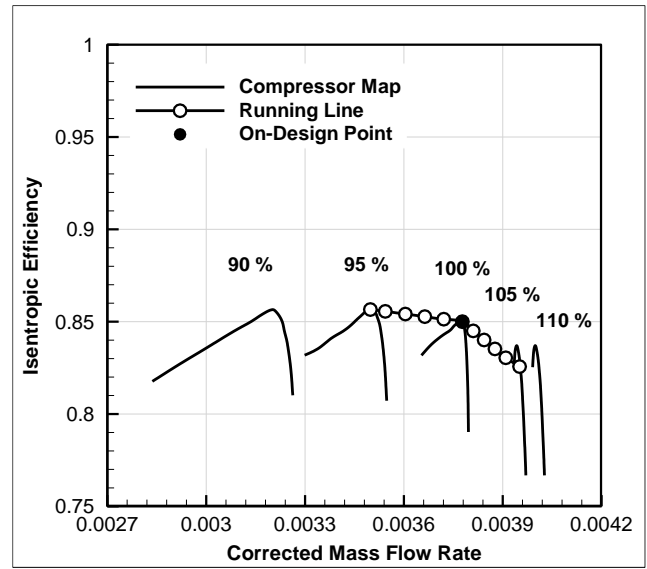


Fig. 26: The on-design and off-design calculation process

The general characteristic diagrams are used for the compressor, turbine, and nozzle characteristic diagrams at the off-design process from 95% to 105% of rotational speed[23, 24]. Considering the Rotor-67 as the first compressor stage, Fig. 27 and Fig. 28 show the running line on the compressor's performance characteristics and turbine, respectively.

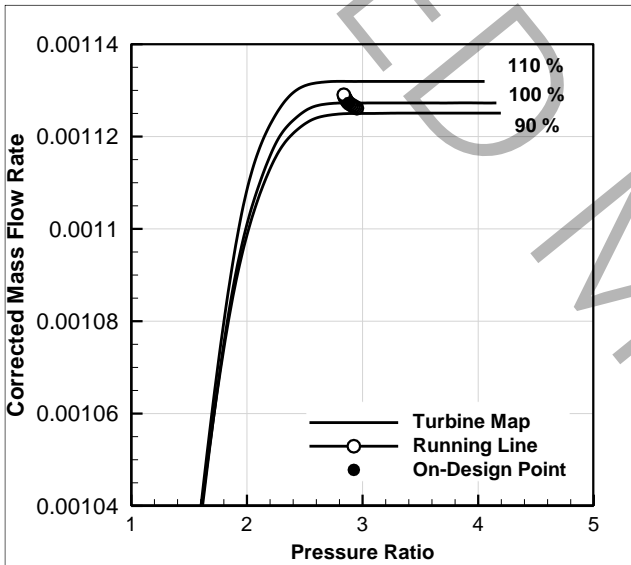


(a)

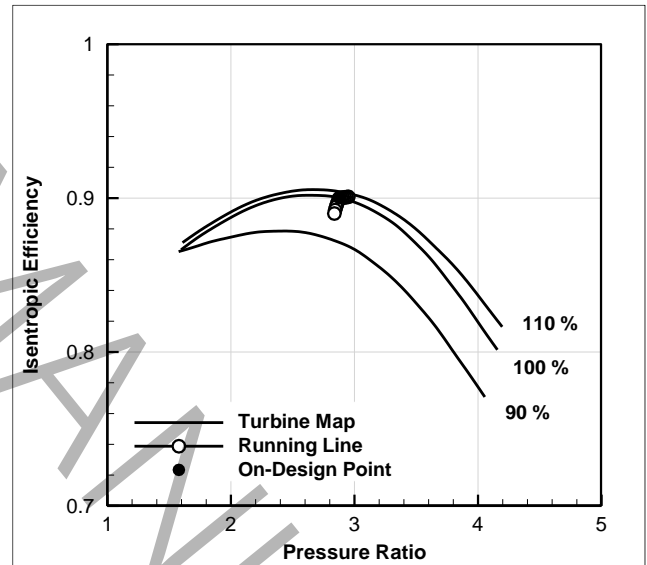


(b)

Fig. 27: The running line on the axial compressor map for (a) corrected mass flow rate-pressure ratio and (b) corrected mass flow rate-isentropic efficiency



(a)

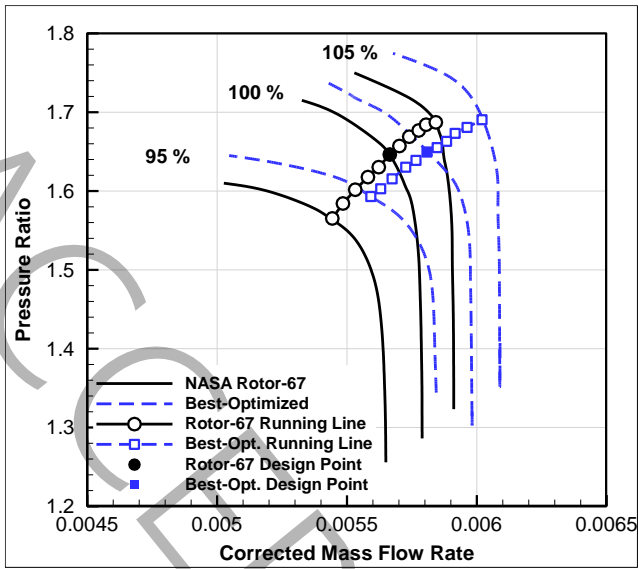


(b)

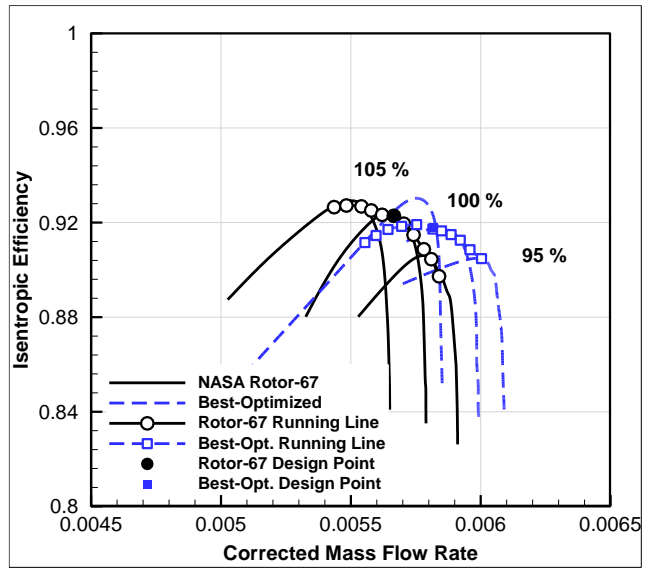
Fig. 28: The running line on the axial turbine map for (a) pressure ratio-corrected mass flow rate and (b) pressure ratio-isentropic efficiency

5-3- Performance Result

A turbojet engine is a machine that consists of the components of the first stage, compressor, turbine, and nozzle. The engine performance analysis is repeated for NASA-Rotor67 and the Best-Optimized rotor as the first stage of the compressor. A comparison of running line results is given in Fig. 29. Also, the Thrust of the turbojet is shown in Fig. 30.



(a)



(b)

Fig. 29: Comparison of the running line of the Best-Optimized rotor with NASA Rotor-67 for (a) pressure ratio-corrected mass flow rate and (b) isentropic efficiency-corrected mass flow rate

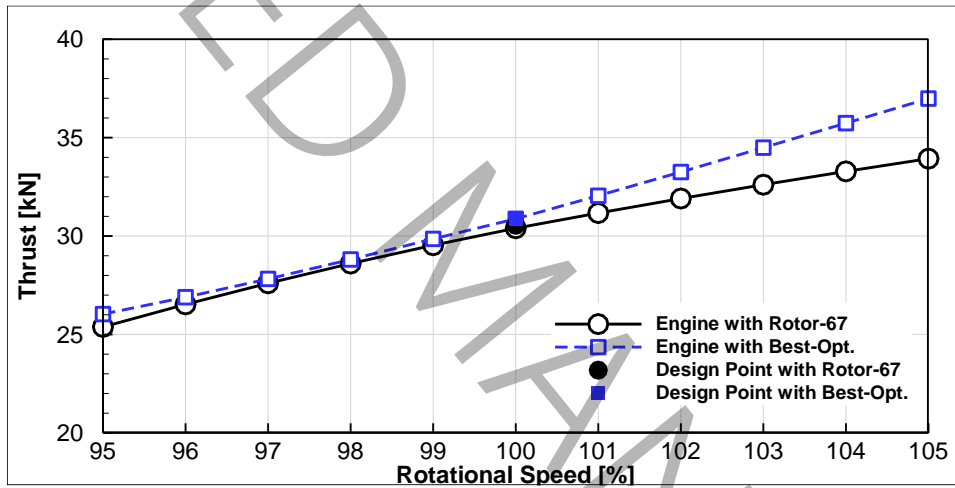


Fig. 30: Comparison of the Thrust of the Turbojet with NASA Rotor-67 and Best-Optimized rotor

The results show that the amount of Thrust has increased in all performance conditions. The percentage of thrust improvement at the design point is equal to 1.57 %.

6- Conclusion

The improve of the axial compressor performance was performed at its characteristic design diagrams. The optimization of the problem was modeled by changing the geometry of the stack-line by two spline curves for lean and sweep at the same time. The compressor has simulated using CFD simulation. This optimal process obtained two geometries optimized at the design point. The best-case results included improved mass flow and pressure ratios of 2.020% and 1.297%, while the isentropic efficiency did not decrease. The improvement of the surge margin is also one of the results obtained after optimization. The trend results of the streamlines behavior show that the negative sweep rotor directs the blade surface shock profile downstream, reduces the pressure loss, and increases the mass flow of the compressor.

Matching turbojet compatibility equations shows that the turbojet engine with Best-Optimized rotor as the first stage of the compressor improves the Thrust at the design point and off-design conditions. The improvement of Thrust is equal to 1.57 % at the design point.

Author Contributions:

Mojtaba Heidarian Shahri: Software, methodology, validation, formal analysis, data curation, investigation, visualization, writing—original draft preparation.

Ali Madadi: Project Administration, supervision, conceptualization, resources, data curation, writing—review and editing.

Romina Ahadian: Software, methodology, validation, formal analysis, data curation, investigation, visualization, writing—original draft preparation.

All authors have read and agreed to the published version of the manuscript.

Funding:

There is no funding for this research.

Data Availability Statement:

Data will be made available on request.

Acknowledgments:

Not applicable.

Declaration of interests:

The authors declare that they have no known competing financial interests or personal relationships that could have appeared to influence the work reported in this paper.

Corresponding author:

Ali Madadi.

7- References

- [1] M.H. Shahri, S. Habibzadeh, A.J.H. Madadi, Three-dimensional optimization of squealer-tip for a transonic axial-flow compressor rotor blade, *Heliyon*, 10(1) (2024).
- [2] M.H. Shahri, S. Habibzadeh, A. Madadi, E.J.A.S. Benini, Technology, Investigation of aerodynamic effects and dominant design variables of cavity squealer-tip in three-dimensional performance of a centrifugal compressor, *Aerospace Science and Technology*, 152 (2024) 109382.
- [3] Z. Wang, F. Qu, Y. Wang, Y. Luan, M.J.E.A.o.C.F.M. Wang, Research on the lean and swept optimization of a single stage axial compressor, *Engineering Applications of Computational Fluid Mechanics*, 15(1) (2021) 142-163.
- [4] T. Eggers, H.R. Kim, S. Bittner, J. Friedrichs, J.R.J.I.J.o.T. Seume, Propulsion, Power, Aerodynamic and aeroelastic effects of design-based geometry variations on a low-pressure compressor, *International Journal of Turbomachinery, Propulsion and Power*, 2020, 5(4) (2020) 26.
- [5] K. Hamaguchi, Y. Sakata, N. Fujisawa, Y. Ohta, D.J.I.J.o.G.T. Kato, Propulsion, P. Systems, Effect of forward-swept rotor on stall margin in an axial flow compressor at distorted inflow condition, *International Journal of Gas Turbine, Propulsion and Power Systems*, 2020, 11(4) (2020) 13-21.
- [6] Z.-l. Li, X.-g. Lu, G. Han, J.-q.J.E.A.o.C.F.M. Zhu, Investigation on flow mechanism of an advanced transonic centrifugal compressor with free-form impeller at design and off-design speeds, *Engineering Applications of Computational Fluid Mechanics*, 2022, 16(1) (2022) 1739-1760.
- [7] E.J.J.o.p. Benini, power, Three-dimensional multi-objective design optimization of a transonic compressor rotor, *Journal of propulsion and power*, 20(3) (2004) 559-565.
- [8] E. Benini, R. Biollo, On the aerodynamics of swept and leaned transonic compressor rotors, in: *Turbo Expo: Power for Land, Sea, and Air*, 2006, pp. 283-291.
- [9] J. Wang, X. He, B. Wang, X.J.J.o.E.f.G.t. Zheng, Power, Shapley additive explanations of multigeometrical variable coupling effect in transonic compressor, *Journal of Engineering for Gas turbines and Power*, 144(4) (2022) 041015.
- [10] M. Heidarian Shahri, A. Madadi, M.J.J.o.A.F.M. Boroomand, Three-dimensional optimization of blade lean and sweep for an axial compressor to improve the engine performance, *Journal of Applied Fluid Mechanics*, 16(11) (2023) 2206-2218.
- [11] A. Sarabchi, M. Heydarian Shahri, A.J.J.o.A.S. Madadi, Technology, A study on lean, sweep and chord length effects on aerodynamic performance of axial fan of a high-bypass ratio turbofan engine, *Journal of Aerospace Science and Technology*, 14(1) (2021) 45-55.
- [12] H. Shahverdi, M. Heidarian Shahri, A. Tebyanian, Y.J.J.o.A.S. Ghobad, Technology, A study on the aeroelastic analysis of AGARD wing in subsonic and transonic flow regimes, *Journal of Aerospace Science and Technology*, (2024).
- [13] A.J. Strazisar, J.R. Wood, M.D. Hathaway, K.L. Suder, Laser anemometer measurements in a transonic axial-flow fan rotor, 1989.
- [14] M. Tasharrofi, M.H. Shahri, A.J.H. Madadi, Three-dimensional design, simulation and optimization of a centrifugal compressor impeller with double-splitter blades, *Heliyon*, (2025).
- [15] K. Ekradi, A.J.E. Madadi, Performance improvement of a transonic centrifugal compressor impeller with splitter blade by three-dimensional optimization, *Energy*, 201 (2020) 117582.
- [16] D. Kamari, M. Tadjfar, A.J.A.S. Madadi, Technology, Optimization of SD7003 airfoil performance using TBL and CBL at low Reynolds numbers, *Aerospace Science and Technology*, 79 (2018) 199-211.
- [17] C. Hah, S. Puterbaugh, A. Wadia, Control of shock structure and secondary flow field inside transonic compressor rotors through aerodynamic sweep, in: *Turbo Expo: Power for Land, Sea, and Air*, American Society of Mechanical Engineers, 1998, pp. V001T001A132.
- [18] J.D. Mattingly, K.M. Boyer, H. von Ohain, *Elements of propulsion: gas turbines and rockets*, American Institute of Aeronautics and Astronautics Reston, VA, 2006.
- [19] H.I. Saravanamuttoo, G.F.C. Rogers, H. Cohen, *Gas turbine theory*, Pearson education, 2001.
- [20] J. Kurzke, I. Halliwell, *Propulsion and power: an exploration of gas turbine performance modeling*, Springer, 2018.

[21] Y.J.I.J.o.E.R. Çengel, Green thermodynamics, 31(12) (2007) 1088-1104.

[22] R. Friedman, Recent trends in aviation turbine fuel properties, 1982.

[23] J. Kruzke, GasTurb 13, Design and Off-Design Performance of Gas Turbines, GasTurb GmbH, Aachen, Germany, 2018.

[24] J. Kurazke, I. Halliwell, Propulsion and Power, An Eploration of Gas Turbine Performance Modeling, Springer International Publishing AG, part of Springer Nature 2018, Cham, Switzerland, 2018.

ACCEPTED MANUSCRIPT